Numerical Simulation of Deceleration of an Axisymmetric Vortex

by

Jorge Manuel Pérez Sánchez

B.S.A.E. University of Southern California (1987)

SUBMITTED IN PARTIAL FULFILLMENT OF THE
REQUIREMENTS FOR THE DEGREE OF
Master of Science
in
Aeronautics and Astronautics
at the
Massachusetts Institute of Technology

May 1989

©1989, Massachusetts Institute of Technology

Signature of Author _____
Department of Aeronautics and Astronautics
May 12, 1989

Certified by _____
Professor Earll M. Murman
Thesis Supervisor, Department of Aeronautics and Astronautics

Accepted by _____
or Harold Y. Wachman
t Graduate Committee

MASSACHUSETTS INSTITUTE OF TECHNOLOGY
JUN 07 1989
LIBRARIES

WITHDRAWN
M.I.T.
LIBRARIES

Aero

Numerical Simulation of Deceleration of an Axisymmetric Vortex

by

Jorge M. Pérez Sánchez

Submitted to the Department of Aeronautics and Astronautics on

12 May 1989

in partial fulfillment of the requirements for the Degree of

Master of Science

in Aeronautics and Astronautics

Abstract

The phenomena associated with the deceleration of an incompressible axisymmetric vortex was numerically studied using a steady-state finite difference inviscid code. By imposing a velocity retardation on the outer boundary of a Rankine-type free vortex (i.e., in the absence of solid boundaries) the characteristics of the flow subjected to an adverse pressure gradient could be studied. The main goal was to assess the relation between the flow parameters and the onset of stagnation at the axis, a possible indicator of vortex bursting. However, convergence of the numerical solution failed before stagnation of the flow on the vortex axis was achieved. Results are presented which show the influence of the amount of velocity retardation (or conversely, pressure gradient), the type of initial axial velocity profile, and the ratio of circumferential to axial velocity at the edge of the core of the vortex.

Thesis Supervisor: Earll M. Murman

Title: Professor of Aeronautics and Astronautics

Acknowledgements

There are many people that I would like to thank for helping me out or for just being there when I needed someone. However, I strongly feel that this space should be reserved for those few who really made the difference.

I am very indebted first of all to my advisor, Professor Earll Murman. He made possible my dream of ever attending one great institution of learning, and was very patient when I did not perform up to his expectations.

I would also like to remember three very special people and fellow students of mine that I felt very attached to, and whom I will always regard with the highest steem. The first is Yannis Kallinderis, now Dr. Kallinderis, who became a true friend of mine and companion. He really made my life so much easier in and out of The Cluster (we will have to go for coffee without each other from now on, man). I also have nothing but sincere gratitude and friendship for Gordon Lam and T. Sean Tavares, both of whom provided me with some great moments during my two-year stay at M.I.T.. I feel sad that I will not be able to enjoy their company in a long time. I thank all three of them for what they meant to me.

I would also like to acknowledge the rest of the students at The Cluster, and in particular the European gang: Gerd Fritsch, Helene Felici, and Andre Saxer.

Finally, but most important of all, I thank my parents for all their support during these last seven years. I owe everything I am to them. And to Ana María, who was always in my mind above anything else. Gracias por todo lo que me has dado y has sido para mí, mi amor.

This research was sponsored by the Office of Naval Research under grant N00014-86-K-0288 monitored by Dr. Spiro Lekoudis.

Contents

List of Figures

Nomenclature

a	vortex core radius
A, D_1, D_2	coefficients of governing equation
$C(\Psi)$	rescaled circulation
$f_{i,j}$	grouping of exact derivatives in governing equation
$H(\Psi)$	total head
K	swirl parameter
K_{crit}	maximum swirl parameter before computational divergence
L	length of computational domain
LL	length of imposed axial velocity defect
p	static pressure
p_{axis}	static pressure on the axis
R	height of computational domain
u	axial velocity
$U_{outer}(x)$	specified axial velocity at outer boundary
U_∞	uniform upstream axial velocity
v	radial velocity
w	circumferential velocity
x	axial coordinate
x_0	axial location around which deceleration is centered
α	inlet axial velocity profile parameter
Γ	circulation
$\delta_{i,j}$	horizontal spacing ratio
ϕ	magnitude of axial velocity defect
ω	relaxation parameter
Ω	angular velocity in solid-body-rotation region
Ψ	streamfunction
ρ	density

σ	radial coordinate
$\tilde{\sigma}$	modified radial coodinate
$\theta_{i,j}$	vertical spacing ratio

Chapter 1
Introduction

Vortex generating devices have found widespread aeronautical application because they provide high maneuverability aircraft with unusual, efficient means of obtaining lift and flow separation control [1]. For example, leading edge vortices are used to develop large lift forces at high angles of attack on delta wings, and they are also present in other important aerodynamic flows such as canard and/or strake generated flows.

However, vortex breakdown or vortex bursting has been observed in these flows under certain conditions which have not been clearly determined. The phenomenon usually results in a partial loss of aerodynamic lift and in unsteady rolling moments caused by the inherent pressure fluctuations. Therefore, prediction of the onset of vortex breakdown is of crucial importance to advanced aerodynamic configurations using vortical flows.

Vortex bursting has been extensively studied since it was first observed more than three decades ago [2]. Experimental evidence indicates that when a translating vortex suffers a strong deceleration, the flow develops a stagnation point on the axis and consequently bursts, usually forming a bubble filled with recirculating fluid, although sometimes an expanded vortex core with a spiral structure may also be found. For most applications, the deceleration of the flow is caused by an adverse pressure gradient, such as the pressure recovery near the trailing edge of a wing or in the exit of an expanding nozzle. Experimental observations on the structure of vortex bursting can be found in Sarpkaya[3,4], Lambourne and Bryer[5], and Payne,

Ng and Nelson[6].

Some of the intricate flow features associated with this phenomenon are poorly understood, and in particular the fundamental question of whether the mechanism involved is viscous or inviscid. As of yet, no conclusive evidence has been drawn from theoretical, experimental, or numerical studies concerning this point.

Within the context of steady flow theory, viscous mechanisms most likely are needed to account for flow reversal inside a closed bubble structure at the axis with a viscous shear layer connecting the outer and inner regions of this bubble. Otherwise there would be no way to establish values for the total head and circulation of the inner flow that depended on the upstream conditions. Furthermore, for an inviscid model, discontinuous solutions would be possible inside the bubble[7], not modeling the true state of affairs. This can be understood better if the flow is assumed to be axisymmetric, for then only a two dimensional plane can be used to describe it in terms of a streamfunction Ψ (see Chapter 2 below). Assuming that the vortex axis is described by the streamline where $\Psi = 0$, the rest of the computational domain can be described by streamlines with positive streamfunction values up to the outer boundary, where $\Psi = \Psi_{max}$. For a steady, inviscid flow, the total head and the circulation are constant on a given streamline, so both variables are defined wherever $0 \leq \Psi \leq \Psi_{max}$.

Consider now the case where stagnation at the axis and flow reversal occur: the $\Psi = 0$ streamline would lift off from the axis to separate the region inside the bubble from the outer flow. One possible way to establish the dependence of H and C on Ψ inside this bubble would be to use the concept of analytic continuation of the functions $H(\Psi)$ and $C(\Psi)$. This would imply that both H and C retain the same functional dependence they had in the region where $\Psi \geq 0$. Since the outer flow has positive Ψ values and both fluids are separated by the streamline where $\Psi = 0$, the streamfunction values inside the recirculating region would be negative. For a

vortex core with inlet solid body rotation and uniform axial flow, we would have (see Chapter 2)

$$\Gamma \sim \Psi \quad for \quad \sigma \leq a$$

where σ is the radial coordinate and a is the radius of the vortex core. Beyond stagnation then, the circumferential profile would apparently show also rotation of the opposite sign since the value of the circulation inside the bubble would be negative. However, Leibovich [8] argues that in steady flow this reversal in the sign of the circumferential velocity is impossible, even if viscosity is allowed, since it would require an unavailable torque to maintain it. This argument is supported by experimental observations that indicate a constancy in the sign of rotation inside the bubble [9]. Hafez and Salas [7] performed inviscid computations beyond stagnation allowing the circulation to reverse sign in the bubble, so the validity of their results is questionable. In this respect it seems that the inviscid equations would not be useful to study the mechanism of vortex breakdown.

However, if only computations with no regions of reversed flow are considered, the total pressure and the circulation values are readily obtained from the upstream conditions and since they are constant on streamlines for inviscid flow, they are defined for the entire domain. To avoid flow reversal the computation would have to be stopped when a stagnation point is found in the axis. Thus, if vortex bursting is assumed to occur when the flow at the axis stagnates, inviscid equations can possibly be used to study the characteristics of the flow leading to the onset of bursting.

It might be argued also that the assumptions of steadiness and axisymmetry do not hold for vortex bursting modelling. Although the phenomenon is not truly steady and the spiral form is encountered more often than the bubble form for delta wings, experimental observations by Sarpkaya[4] and Payne, Ng, and Nelson[6], in both water and air, indicate that for sufficiently high flow speeds and swirl, the structure becomes a symmetric bubble and the wandering of the latter about a mean

axial position ceases. The experiments showed that this occurred for Re$\sim$ 425000 in air (based on a root chord of 40.6cm for a delta wing). Sarpkaya[4] also observed that the fluid in the bubble was constantly being replenished and discharged through an opening in the aft portion, which is an indication of strong unsteadiness; however, he concludes that this is caused by instabilities in the wake of the bubble leading to pressure fluctuations. Since our computations would proceed only up to the point of stagnation, no wake effects are present and thus the major source of unsteadiness discarded. Finally, Leibovich[8] noticed that the motion in the inner recirculation zone was unsteady, but with low frequency fluctuations.

The above observations indicate that the bubble is not a closed structure, so the possibility exists that viscous effects are not essential for the bubble's formation, since both the outer and inner flows would originate at regions upstream where the streamfunction Ψ is positive. The two flows would then be connected through the aft section opening of the bubble. However, it is doubtful that this fact could be used in an inviscid numerical simulation to compute the inner flow, because unless stagnation occurs at a point on the axis other than the outflow station of the computational domain, the connection cannot be established between the two flows. Even if stagnation takes place upstream of the outflow boundary, it is not clear how to impose that the rear opening of the bubble lie within the computational boundaries (otherwise the flows are still unconnected). Therefore, it seems again that the computation should not proceed beyond stagnation.

It is the purpose of this research to study the parameters that govern the deceleration of an axisymmetric vortex, ideally leading to the onset of vortex breakdown, using an inviscid code in order to learn about the controlling factors that cause the flow to stagnate at the axis. In this way, results can be developed for comparison with other Euler and Navier-Stokes computational results. Furthermore, the usefulness of an inviscid solution to predict bursting can be evaluated by observing its convergence behavior near stagnation conditions. As with boundary layer codes

that fail to give an answer when flow separation takes place, it is possible that an inviscid code would fail to give a converged solution when stagnation is reached.

In a steady-state, incompressible, inviscid model, there is no mechanism to induce vortex breakdown unless the flow is subjected to a pressure gradient, as can be deduced from the associated Euler equations in the absence of gravity or electromagnetic fields. It follows that we will use the equivalent mechanism of velocity retardation of the outer inviscid flow to induce a wake-like profile near the axis. The characteristics of this deceleration will be gradually modified to assess the relative importance of each one of the parameters involved.

The deceleration parameters used in this study are: (1) the magnitude of the velocity retardation at the outer boundary, and (2) the length over which the deceleration takes place. The axial location at which the deceleration region is centered is also considered to assess the effect of the inflow and outflow boundary conditions on the results. The main controlling factor for a given inlet velocity profile is the ratio of maximum circumferential to axial velocity, called the swirl parameter K.

Thus, if the length and magnitude of the deceleration are constant, the swirl can be increased until it reaches a (maximum) critical value for which a converged numerical solution ceases to exist.

A family of velocity profiles was used that resemble experimentally observed swirling flows in different fields of applications [10]. As an interesting case, a self-similar conical solution to the viscous Navier-Stokes equations obtained by Powell[11] was also used as an input to the inviscid model.

Chapter 2

Governing Equation and Boundary Conditions

The governing equation used in this study is a modified incompressible, inviscid vorticity transport equation in cylindrical coordinates (σ, θ, x) with velocity components (v,w,u), adapted for axisymmetric flows (i.e., no θ-dependence). The axisymmetric character of the flow allows us to consider just a two dimensional plane defined by θ =constant and obtain the governing equation in terms of a streamfunction Ψ, where

$$u = \frac{1}{\sigma}\frac{\partial \Psi}{\partial \sigma} \quad , \quad v = \frac{-1}{\sigma}\frac{\partial \Psi}{\partial x}. \tag{2.1}$$

The total head H and modified circulation C of the flow are defined as functions of Ψ

$$\begin{aligned} H(\Psi) &= \tfrac{1}{2}(u^2 + v^2 + w^2) + \tfrac{p}{\rho} \\ C(\Psi) &= \sigma w = \tfrac{\Gamma}{2\pi} \end{aligned} \tag{2.2}$$

where Γ is the circulation. Then, the governing equation is simply obtained from the definition of the vorticity components ω_θ, ω_σ, and ω_x as

$$\frac{\partial^2 \Psi}{\partial x^2} + \frac{\partial^2 \Psi}{\partial \sigma^2} - \frac{1}{\sigma}\frac{\partial \Psi}{\partial \sigma} = \sigma^2 \frac{dH}{d\Psi} - C\frac{dC}{d\Psi}. \tag{2.3}$$

Equation (2.3) is derived in detail in reference [12].

At the upstream boundary the assumption of radial equilibrium, i.e. the pressure is balanced by the centrifugal acceleration, is used to give

$$H(\Psi) = \frac{1}{2}(u^2 + v^2 + w^2) + \int_0^\sigma \frac{C^2}{\xi^3} d\xi + \left(\frac{p}{\rho}\right)_{axis}. \tag{2.4}$$

Since the streamfunction values are derived from the axial velocity profile at this boundary, it is possible to determine the values of C and H as functions of Ψ there. Furthermore, C and H will be constant for a given streamline due to the inviscid assumption, so if the value of the streamfunction is given anywhere in the flow, the values for the total head and circulation can be readily obtained at that point using interpolation.

2.1 Boundary Conditions

Since the flow is axisymmetric, the computational domain is taken as the rectangle formed by the vortex axis at the lower boundary ($\sigma = 0$), the upper radial boundary ($\sigma = R$), the inflow plane ($x = 0$), and the outflow plane ($x = L$). The upstream or inflow boundary conditions are determined by the following velocity profiles, used in reference [10]:

$$\frac{u(\sigma)}{U_\infty} = \begin{cases} \alpha + (1-\alpha)\sigma^2(6 - 8\sigma + 3\sigma^2) & \text{if } \sigma \leq a \\ 1 & \text{if } \sigma \geq a \end{cases}$$

$$\frac{w(\sigma)}{U_\infty} = \begin{cases} \Omega\sigma & \text{if } \sigma \leq a \\ \frac{\Omega a^2}{\sigma} & \text{if } \sigma \geq a \end{cases} \tag{2.5}$$

i.e. $\sigma = a$ is the core of the vortex, defined as the radial location up to which the circumferential profile consists of a solid-body rotation with angular speed Ω. The outer portion is a potential vortex. The parameter α in the axial velocity is used to establish a uniform profile of magnitude U_∞ ($\alpha = 1$), a wake-like profile of minimum velocity αU_∞ at the axis ($\alpha < 1$), or a jet-like of maximum velocity αU_∞ at the axis ($\alpha > 1$). In typical aeronautical applications, the axial profile presents a jet at the core region (corresponding to $\alpha > 1$), and a circumferential velocity profile

which can be approximated by a Rankine-type vortex (which is modeled by the profile used in this study). Integration of the axial velocity profile using (2.1) gives the upstream boundary condition in terms of streamfunction Ψ

$$\Psi = \begin{cases} U_\infty \sigma^2 \{\frac{\alpha}{2} + (1-\alpha)[\frac{3}{2} - \frac{8}{5}\sigma + \frac{1}{2}\sigma^2]\sigma^2\} & \text{if } \sigma \leq a \\ U_\infty \{\frac{\sigma^2}{2} + 0.1(\alpha - 1)\} & \text{if } \sigma \geq a. \end{cases} \tag{2.6}$$

Note that this imposes no value on the radial velocity v.

The condition at the upper boundary is simply the imposed retardation function $U_{outer}(x)$ which defines the velocity along that boundary. The functional form of the retardation itself is given by

$$U_{outer}(x) = \begin{cases} U_\infty & \text{x} < (x_0 - \frac{LL}{2}) \\ U_\infty \{1 + \frac{\phi}{2}[\cos\left(\frac{x - x_0 + LL/2}{LL/\pi}\right) - 1]\} & (x_0 - \frac{LL}{2}) \leq x \leq (x_0 + \frac{LL}{2}) \\ U_\infty (1 - \phi) & \text{x} > (x_0 + \frac{LL}{2}) \end{cases} \tag{2.7}$$

where ϕ is the magnitude of the velocity decrease as a fraction of the velocity at upstream infinity; x_0 is the location around which the deceleration is centered; and LL is the length over which the deceleration takes place. A typical outer boundary velocity function is shown below in Fig. 2.1 for the case x_0 =L/2 and LL=3.0, with a deceleration $\phi = 0.5$. The specification of the velocity at the outer boundary in turn determines the value of $\left(\frac{\partial \Psi}{\partial \sigma}\right)_{outerboundary}$, which may be discretized and used in the computation. See Chapter 4 for details of the implementation.

The lower boundary condition imposed on the vortex axis is given by

$$\Psi = 0 \tag{2.8}$$

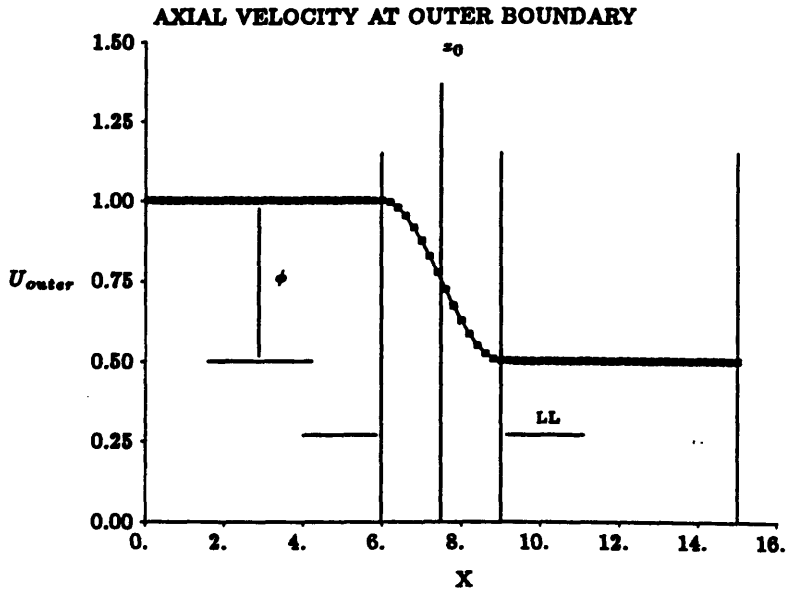

Figure 2.1: Typical outer boundary imposed velocity function

ensuring that the axis is always a streamline of the flow and therefore that the radial velocity on it is zero. The outflow boundary condition requires that the flow does not change with the axial direction in exiting the domain, i.e.

$$\frac{\partial \Psi}{\partial x} = 0. \tag{2.9}$$

The imposition of parallel flow boundary conditions at the exit plane of the domain is a reasonable choice. A specified velocity or pressure field could have also been used but it is uncertain that these would produce meaningful results without knowing the outflow conditions *a-priori*. Imposition of (9) assures that the behavior of the flow is completely determined within the domain boundaries, and that no developments further downstream need be considered. However, the question arises as to whether this condition actually hinders or encourages bursting behavior in the flow.

Chapter 3
Normalization

The following parameters were used to render the governing equation dimensionless:

$$\begin{aligned} \overline{u},\overline{v},\overline{w} &= \tfrac{u,v,w}{U_\infty} \quad , \quad \overline{x},\overline{\sigma} = \tfrac{x,\sigma}{a} \\ \overline{\Psi} &= \tfrac{\Psi}{U_\infty a^2} \\ \overline{H} &= \tfrac{H}{U_\infty^2} \quad , \quad \overline{C} = \tfrac{C}{aU_\infty}. \end{aligned} \tag{3.1}$$

Normalizing with the above parameters leaves the governing equation (2.3) unchanged. Both the upstream and the upper boundary conditions for $\Psi(\sigma)$ drop the factor U_∞, while the expressions for the total head H and the modified circulation C at the inflow boundary become

$$\overline{H} = \begin{cases} 1/2\{\alpha + (1-\alpha)\overline{\sigma}^2(6 - 8\overline{\sigma} + 3\overline{\sigma}^2)\}^2 + (K\overline{\sigma})^2 & \text{if } \overline{\sigma} \le 1 \\ 1/2 + K^2 & \text{if } \overline{\sigma} \ge 1 \end{cases}$$

$$\overline{C} = \begin{cases} K\overline{\sigma}^2 & \text{if } \overline{\sigma} \le 1 \\ K & \text{if } \overline{\sigma} \ge 1 \end{cases} \tag{3.2}$$

where the dimensionless parameter K is the swirl parameter defined as

$$K = \frac{\Omega a}{U_\infty}$$

or the ratio of circumferential to axial velocity at the vortex core edge in the inflow plane. Notice that the core edge is now at a unit distance from the axis at the inflow station, and that the domain dimensions are all in units of vortex core radii. The

flow now has unit velocity at upstream infinity and the deceleration will simply be of magnitude ϕ.

The pressure term $\frac{p}{\rho}$ is also normalized using ${U_\infty}^2$, and is equal to

$$\overline{p} = \overline{H} - \frac{1}{2}\left(\overline{u}^2 + \overline{v}^2 + \overline{w}^2\right). \tag{3.3}$$

Notice then that the normalized pressure at the axis is equal to the difference of total head and axial velocity term there since radial and circumferential velocities vanish on the axis. Recall from Chapter 2 that the radial equilibrium assumption used at the upstream boundary results in the following expression for the pressure

$$\overline{p} = \int_0^{\overline{\sigma}} \frac{\overline{C}^2}{\overline{\xi}^3} d\overline{\xi} + \overline{p}_{axis}. \tag{3.4}$$

In this study $\overline{p}_{axis}$ is taken to be zero for the sake of simplicity.

Chapter 4

Discretization and Method of Solution

Designating points in the x and σ directions with i and j subscripts respectively, the discretization of equation (2.3) gives

$$\left\{\frac{\delta_{ij}\Psi_{i+1,j}-(1+\delta_{ij})\,\Psi_{ij}+\Psi_{i-1,j}}{\frac{1}{2}\left[\delta_{ij}\,(x_{i+1}-x_i)^2+(x_i-x_{i-1})^2\right]}\right\}$$

$$+\left\{\frac{\theta_{ij}\Psi_{i,j+1}-(1+\theta_{ij})\,\Psi_{ij}+\Psi_{i,j-1}}{\frac{1}{2}\left[\theta_{ij}\,(\sigma_{j+1}-\sigma_j)^2+(\sigma_j-\sigma_{j-1})^2\right]}\right\}$$

$$-\frac{1}{\sigma_j}\left\{\frac{{\theta_{ij}}^2\Psi_{i,j+1}+\left(1-{\theta_{ij}}^2\right)\Psi_{ij}-\Psi_{i,j-1}}{(\sigma_j-\sigma_{j-1})+{\theta_{ij}}^2\,(\sigma_{j+1}-\sigma_j)}\right\}$$

$$=\left\{\sigma_j^2\left(\frac{dH}{d\Psi}\right)_{ij}-\left(C\frac{dC}{d\Psi}\right)_{ij}\right\} \tag{4.1}$$

where the following variables have been used for simplification

$$\begin{aligned}\theta_{ij} &= \left[\frac{\sigma_j-\sigma_{j-1}}{\sigma_{j+1}-\sigma_j}\right]_i\\ \delta_{ij} &= \left[\frac{x_i-x_{i-1}}{x_{i+1}-x_i}\right]_j.\end{aligned} \tag{4.2}$$

At the boundaries it is assumed that the mesh spacings are equal on both sides, so that $\theta_{ij_{max}}=1$ and $\delta_{i_{max}j}=1$. The discretization errors incurred through this scheme are of the order

$$\max\left\{(\sigma_{j+1}-\sigma_j)^2,(\sigma_j-\sigma_{j-1})^2,(x_{i+1}-x_i)^2,(x_i-x_{i-1})^2\right\}$$

for the whole domain.

The Line-SOR method is an implicit scheme where an attempt is made to obtain the value of Ψ at three consecutive points of the mesh simultaneously. In this study the points are taken from horizontal rows, so solving for $\Psi_{i-1,j}$, Ψ_{ij}, and $\Psi_{i+1,j}$ we get

$$A\Psi_{i+1,j} + \Psi_{i,j} + A\Psi_{i-1,j} = A\left\{f_{i,j} - D_1\Psi_{i,j-1} - D_2\Psi_{i,j+1}\right\} \tag{4.3}$$

where the following coefficients have been introduced, assuming that the mesh spacing in the axial direction is constant (i.e. $\delta_{ij} = 1$, and $\Delta x = x_{i+1} - x_i$)

$$f_{i,j} = \left\{\sigma_j^2\left(\frac{dH}{d\Psi}\right)_{ij} - \left(C\frac{dC}{d\Psi}\right)_{ij}\right\}(\Delta x)^2$$

$$A = \left\{\frac{-1/(\Delta x)^2}{\frac{2}{(\Delta x)^2} + \frac{2(1+\theta_{ij})}{\left[\theta_{ij}(\sigma_{j+1}-\sigma_j)^2+(\sigma_j-\sigma_{j-1})^2\right]} + \frac{(1-\theta_{ij}{}^2)}{\sigma_j\left[\sigma_j-\sigma_{j-1}+\theta_{ij}{}^2(\sigma_{j-1}-\sigma_j)\right]}}\right\}$$

$$D_1 = (\Delta x)^2\left\{\frac{2}{\theta_{ij}(\sigma_{j+1}-\sigma_j)^2 + (\sigma_j-\sigma_{j-1})^2} + \frac{1}{\sigma_j\left[\sigma_j-\sigma_{j-1}+\theta_{ij}{}^2(\sigma_{j+1}-\sigma_j)\right]}\right\}$$

$$D_2 = (\Delta x)^2\left\{\frac{2\theta_{ij}}{\theta_{ij}(\sigma_{j+1}-\sigma_j)^2 + (\sigma_j-\sigma_{j-1})^2} - \frac{\theta_{ij}{}^2}{\sigma_j\left[\sigma_j-\sigma_{j-1}+\theta_{ij}{}^2(\sigma_{j+1}-\sigma_j)\right]}\right\}.$$

If we now take these three Ψ values at the $(n+1)^{th}$ iteration and subtract the old values of the n^{th} iteration using

$$\Delta\Psi_{ij}{}^{n+1} = \Psi_{ij}{}^{n+1} - \Psi_{ij}{}^{n}$$

we obtain the delta form of the discretized governing equation

$$A\Delta\Psi_{i+1,j}{}^{n+1} + \Delta\Psi_{i,j}{}^{n+1} + A\Delta\Psi_{i-1,j}{}^{n+1} =$$
$$A\left\{f_{i,j}{}^{n} - D_1\Psi_{i,j-1}{}^{n+1} - D_2\Psi_{i,j+1}{}^{n}\right\} - A\Psi_{i+1,j}{}^{n} - \Psi_{i,j}{}^{n} - A\Psi_{i-1,j}{}^{n}. \qquad (4.4)$$

Notice that $f_{i,j}$ represents the right hand side of (4.1), and it contains head and circulation terms (including derivatives). To find these terms, the most recent value of Ψ at the point $\{i, j\}$ is used to determine H(Ψ) and C(Ψ) from linear interpolation using the values at the upstream boundary . At each step of the computation these terms are frozen, and their derivatives computed using $\Psi_{i,j-1}{}^{n+1}$, $\Psi_{i,j}{}^{n}$, and $\Psi_{i,j+1}{}^{n}$.

The Line-SLOR method updates the value of Ψ in all the discretized points of the rectangular domain except those lying on the axis (lower boundary) and those on the inflow boundary, where Dirichlet boundary conditions are prescribed. At the other two boundaries Neumann conditions are implemented, as explained in Section 2.1. Therefore, if we designate the right hand side of the discretized delta-form equation (4.4) as F_{ij} and write the equation for each point of a horizontal row excluding those on the lower and inflow boundaries, we can write the resulting system of discretized equations in matrix form as

$$\begin{bmatrix} 1 & A & & \cdots & & & 0 \\ A & 1 & A & & & & \\ & \ddots & \ddots & \ddots & & & \\ & & & & & & \\ & & & & & & \\ & & & \ddots & \ddots & \ddots & \\ & & & & A & 1 & A \\ 0 & & & \cdots & & 2A & 1 \end{bmatrix} \begin{bmatrix} \Delta\Psi_{2j} \\ \Delta\Psi_{3j} \\ \vdots \\ \\ \\ \vdots \\ \Delta\Psi_{Imax-1,j} \\ \Delta\Psi_{Imax,j} \end{bmatrix} = \begin{bmatrix} F_{2j} \\ F_{3j} \\ \vdots \\ \\ \\ \vdots \\ F_{Imax-1,j} \\ F_{Imax,j} \end{bmatrix}.$$

Notice that the outflow boundary condition $\frac{\partial \Psi}{\partial x} = 0$ has been implemented in the last row of the matrix through the discretization of (2.9) in 2.1. The outer boundary condition (2.7) is implemented by first writing the discretized version of the definition of streamfunction, equation (2.1), as

$$U_{ij} = \frac{(\Psi_{i,j+1} - \Psi_{i,j-1})}{\sigma_j(\sigma_{j+1} - \sigma_{j-1})}. \tag{4.5}$$

If we now apply this discretization at the outer boundary, the term in the left hand side is the imposed axial velocity given by equation (2.7), and the subscripts change from j to j_{max} since $\sigma_{i,j_{max}} = R$ is the location of the boundary. That is,

$$U_{outer}(R, x_i) = \frac{(\Psi_{j_{max}+1} - \Psi_{j_{max}-1})_i}{\sigma_{j_{max}}(\sigma_{j_{max}+1} - \sigma_{j_{max}-1})}. \tag{4.6}$$

Notice that since the left hand side is a known function, the equation can be solved for $\Psi_{i,j_{max}+1}$ and this relation used to obtain an expression for the discretized first and second order partial derivatives, $\left(\frac{\partial \Psi}{\partial \sigma}\right)_{i,j_{max}}$ and $\left(\frac{\partial^2 \Psi}{\partial \sigma^2}\right)_{i,j_{max}}$, to be used in the governing equation. It is also assumed that at the upper boundary $\sigma_{j_{max}} - \sigma_{j_{max-1}} = \sigma_{j_{max+1}} - \sigma_{j_{max}}$.

Since there is one matrix for each horizontal row of discrete points, the number of matrix inversions will equal the number of rows in the domain. Solving this matrix equation will give the values $\Delta {\Psi_{ij}}^{n+1}$ to be used in the relaxation equation

$${\Psi_{ij}}^{n+1} = {\Psi_{ij}}^{n} + \omega \Delta {\Psi_{ij}}^{n+1} \tag{4.7}$$

where the last term is the residual of the computation (i.e. the difference between new and old values). The method is used iteratively, updating the values of Ψ_{ij} in the entire domain at each iteration. Convergence of the solution is assumed when the value of the residual falls below 10^{-5} . In the study, both overrelaxation ($\omega > 1$) and underrelaxation ($\omega < 1$) were used, the latter being necessary when the

solution approached stagnation ($\omega \sim 0.6$). The high non-linearity of the problem made impractical the implementation of numerical schemes to optimize the value of the relaxation parameter ω at each iteration.

Near stagnation conditions, application of (4.7) would often result in negative values of Ψ near the axis during the iterative process, requiring the computation to utilize values for the total head H and circulation C that were undefined. To avoid this problem, Ψ was set to zero at these points before proceeding to the next iteration.

Chapter 5
Computation

Equation (2.3) was discretized and solved using the implicit Successive Line Over-Relaxation Method (SLOR) in delta-form, described in Chapter 4. This scheme has the advantage that boundary conditions are easily implemented through the delta-form.

An algebraically generated grid was used in this computation, with clustering of discrete points in the vertical direction near the vortex axis according to the following rule:

$$\tilde{\sigma} = R\left\{\frac{\log[\sigma+1]}{\log[R+1]}\right\}^n \tag{5.1}$$

where n is the clustering controlling parameter ($n > 2$), taken to be 2.2 in this study. Larger values of n will result in higher point densities near the axis, but the value used was found to be adequate for our purposes and the results did not differ appreciably from those obtained using higher n values. The grid is shown in Fig. 5.1 for a $61x31$ point mesh.

5.1 Effect of Computational Parameters

Several trial runs were performed to assess the dependence of results on the domain dimensions. Both the length L and the height R were increased with all

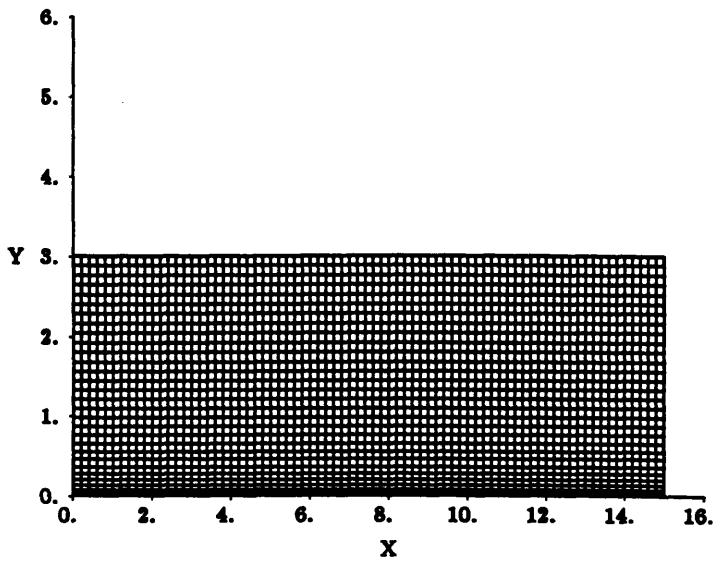

Figure 5.1: Plot of typical 61x31 point mesh used in the computations

other parameters fixed until the solution remained essentially constant. The fixed values used were K= 0.7, $\phi = 0.2$, $\alpha = 1.0$, and LL= 2.0. It was found that for a typical 61x31 mesh, L=15 was a suitable value since further increase in this length resulted in variations in converged solutions of less than $\pm 0.7\%$.

It was also found that convergence of the computation was much slower as R increased than with equal increments in L. This was due to the fact that the Line-SOR method used horizontal or row sweeping, so that the number of matrix inversions increased with the number of points in the vertical direction.

Using fixed values of axial length L, deceleration length LL, and swirl K, the radius R and the deceleration magnitude ϕ can be varied in such a way that the axial velocity at the edge of the vortex-core at the outflow boundary remains constant. In this way, cases with different values of R can be rescaled by changing K and ϕ. Therefore the choice of domain height is governed solely by the need to minimize vertical space (upper R bound) while allowing the core to expand fully inside the domain boundaries as it is decelerated (lower bound). A value R=3 was selected. Although this value did not allow the core to expand fully for cases with $\phi \geq 0.8$, it

was considered appropriate since increasing the value of R further led to very lengthy calculations and it presented no problems for all but two of the cases considered: $\phi = 0.8, 0.9$.

It was also found that cell aspect ratios around 2 near the axis were appropriate to ensure good resolution with a minimum of points in the horizontal direction. Cell aspect ratios of 1 and 4 were also considered, showing that the finer resolution in the σ direction gives results closer to those obtained using overall (i.e. in both directions) finer grids.

The length of deceleration and the location around which it was centered were also varied. The results indicate that the location is of minor importance as long as it is not too close to the outflow boundary. This is because the outflow boundary condition (2.9) requires the flow variables to be independent of the axial coordinate, remaining unchanged after reaching the exit plane. Similarly, the length over which the retardation takes place has no effect on the final results if the above criterion is applied. This implies in turn that the final configuration of the flow is insensitive to the way in which the deceleration has been brought about. Thus, the computations were all performed using a length of retardation LL=3 centered around L/2.

A deceleration followed by an acceleration of the flow was also considered, especially to achieve near zero axis velocities in cases where previously this was not possible (large K computations). Ideally, the flow at the stagnation region would be less affected by the outflow boundary condition due to the buffer effect provided by the acceleration region. The longer the middle region between deceleration and acceleration, the better the original flow would be modeled. However, this arrangement proved impractical because this middle region had to be quite long to faithfully model original conditions, and eventually the computations were equally slow, diverging as stagnation was approached.

5.2 Verification

The solution to the case of swirling flow with uniform inlet axial profile inside a tube subjected to a gradual area expansion has been solved analytically by Batchelor [12]. A comparison between his solution and the numerical computations was made using the fact that if the expansion of the streamlines is known, then the flow inside any streamsurface is essentially a tube flow. The results for $\phi = 0.2$ and K= 0.5 are compared in Figs. 5.2 and 5.3 below for the flow delimited by the core edge streamline, showing good agreement. Both axial velocity and circumferential velocity profiles are compared.

It was found that the computational solution approached the analytical solution as the number of discrete points increased, especially near the axis and the vortex core edge. For example, the slight discrepancy observed in the minimum axial velocity in Fig. 5.2 is due to the fact that the value of the axis velocity strongly depends on the magnitude of core edge expansion, and in a discretized model an error is introduced since the location of the core edge is approximated by the nearest discrete point.

5.3 Computational Studies

A series of computational studies were done to determine the effect of various parameters on the onset of vortex breakdown. The computation started with fixed values of deceleration at the outer boundary (given by ϕ) and inlet axial profile (α). It then proceeded with increasing values of swirl parameter K until a solution could not be obtained. The results shown in this study correspond to computations using $\alpha = (1, 1.2, 0.8)$ and $\phi = \{0.1 \longrightarrow 0.9\}$. Convergence was assumed when the residual fell below 10^{-5}.

The computations were run on a MicroVax computer. Typical CPU times for critical cases were around 45 minutes, and a typical number of iterations was 3400 for a 61x31 point grid.

As a test for comparison, Powell's self-similar conical solution of the Navier-Stokes equations [11] was used as an input to our inviscid model, taking his axial and circumferential velocities, and total pressure and circulation, as the new upstream boundary conditions. To obtain a meaningful comparison, a conical solution with an axial velocity profile similar to an $\alpha = 1.2$ case was employed. However, this implied that the circumferential velocity and total pressure profiles would be already determined as part of the conical solution, without the possibility to make them approximate our profiles.

Since the normalization of the equations required a characteristic length, and since a vortex core radius a was not defined for Powell's solution, use was made of the radial coordinate value at which the circumferential velocity was largest. The characteristic velocity for normalization was taken to be the axial velocity at the outer edge of the vortex. In this way the normalization of the new boundary condition was consistent with the normalization of the governing equation and the other boundary conditions.

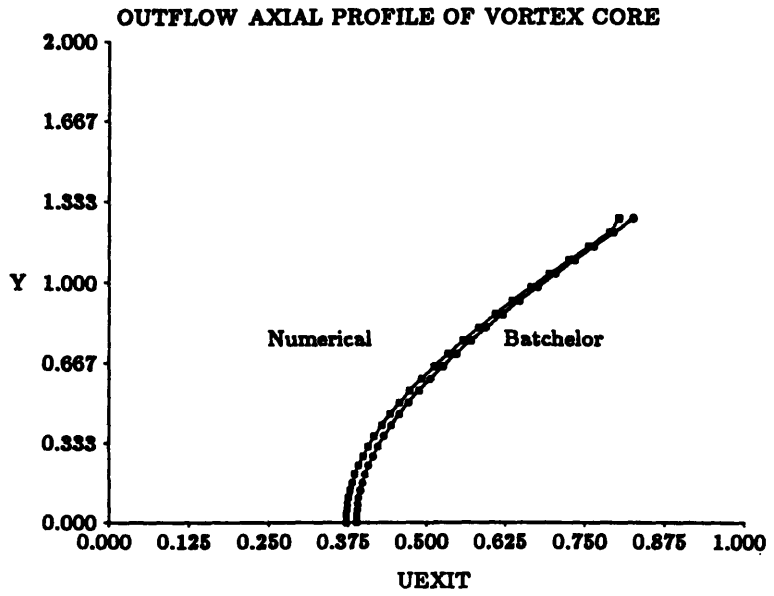

Figure 5.2: Axial Profile Comparison with Batchelor: $\phi = 0.2$, K= 0.5, $\alpha = 1$

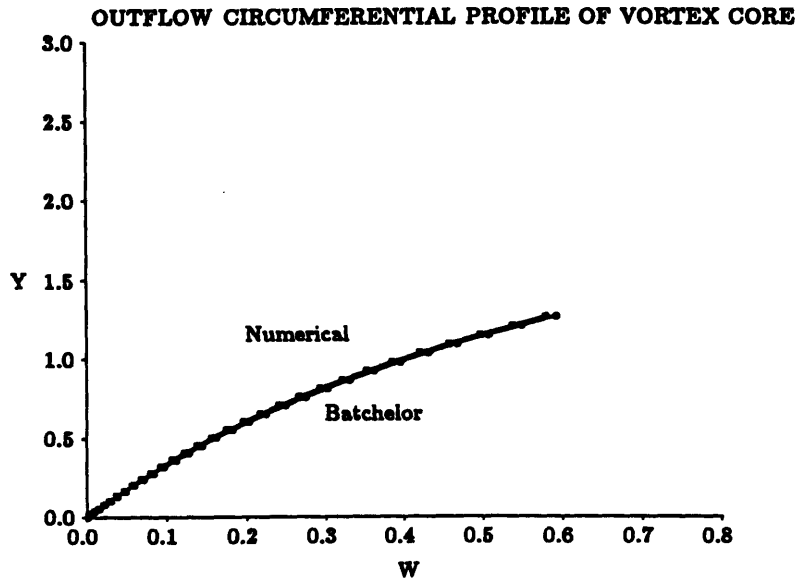

Figure 5.3: Circumferential Profile Comparison with Batchelor: $\phi = 0.2$, K= 0.5, $\alpha = 1$

Chapter 6

Results

6.1 Case I: $\alpha = 1$

Consider a typical solution given by a deceleration $\phi = 0.1$ and the other parameters fixed as discussed in Chapter 5. The swirl K was increased in order to decelerate the flow near the axis and drive it to stagnation. The results of this deceleration are shown below in Figs. 6.1, 6.2, 6.3, and 6.4, where plots of streamlines, axial velocity, circumferential velocity, and static pressure are presented.

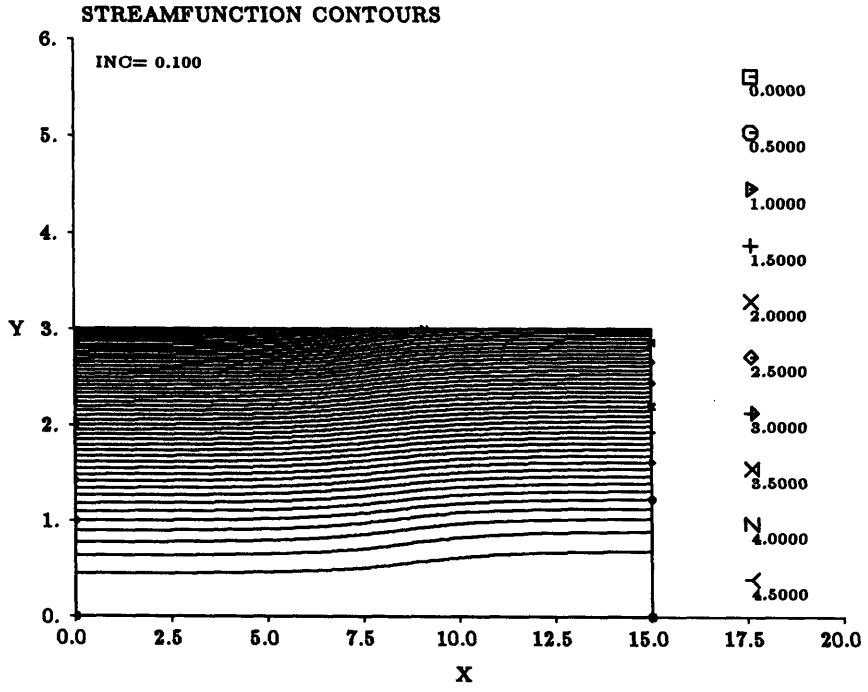

Figure 6.1: Streamfunction Contours, Critical case:$\phi = 0.1, \alpha = 1.0, K = 0.936$

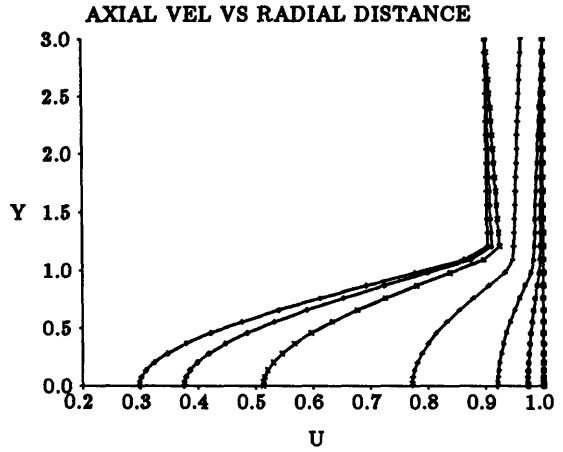

Figure 6.2: Axial profiles, Critical case:$\phi = 0.1, \alpha = 1.0, K = 0.936$

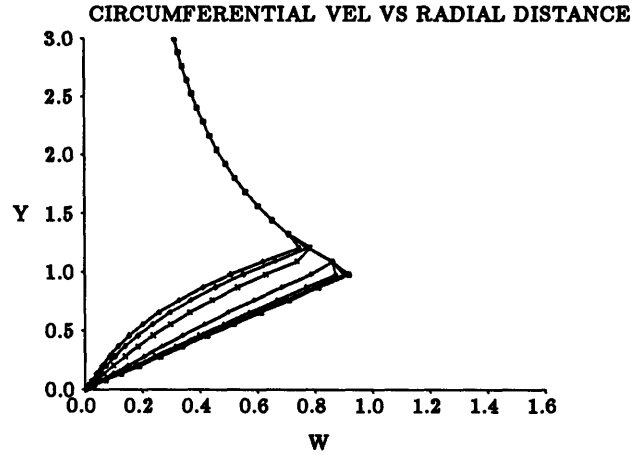

Figure 6.3: Circumf profiles, Critical case:$\phi = 0.1, \alpha = 1.0, K = 0.936$

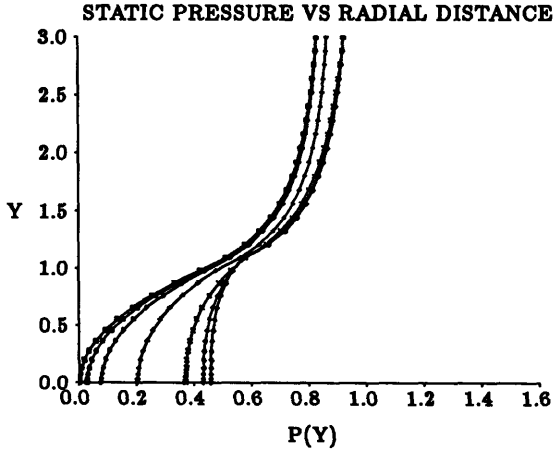

Figure 6.4: Static pressure, Critical case:$\phi = 0.1, \alpha = 1.0, K = 0.936$

Each of the last three figures shows seven curves corresponding to data at seven axial locations along the domain length L: inlet (x= 0), x=L/4, x=3L/8, x=L/2, x=5L/8, x=3L/4, and exit station (x=L). In the axial velocity plot, the rightmost curve corresponds to x=0, and the leftmost curve to x=L. In the circumferential velocity plot, the solid body rotation core profile corresponds to the inlet station. Finally, in the static pressure plot, the leftmost curve represents values at the inflow, and the rightmost curve values at the outflow. Notice that since the chosen length of retardation is LL=3 centered around L/2, only one station will be inside the deceleration region.

Fig. 6.1 shows an expansion of the vortex core as the flow is retarded, with some of the streamlines leaving the domain through the outer (upper) boundary to satisfy conservation of mass. In Fig. 6.3 it is clearly seen that the circumferential velocity profile is also altered by the deceleration, and its maximum value decreases to satisfy conservation of angular momentum. The static pressure increases throughout the domain, as can be expected from the fact that the flow is expanding. Notice from Fig. 6.2 that the minimum axial velocity obtained is not zero. The computation failed to give a converged solution for higher values of swirl K, in what would be a typical behavior of the computation for many cases. A typical convergence history of a converged solution is shown in Fig. 6.11 below.

Thus, although the goal of the computation was to determine the onset of vortex bursting by studying the flow near stagnation conditions, in some cases it was not possible to obtain a converged solution for which the axis velocity approached zero. This was especially true for cases of small retardation values (large critical swirl parameter K_{crit}). Table 6.1 below shows the minimum velocity values obtained in this study for different values of ϕ, together with values of the corresponding K_{crit}. It can be observed that only for cases of strong deceleration the minimum velocity approached zero.

ϕ	$U_{minimum}$	K_{crit}
0.1	0.308	0.936
0.2	0.188	0.779
0.3	0.132	0.652
0.4	0.120	0.538
0.5	0.035	0.434
0.6	0.019	0.339
0.7	0.0077	0.249
0.8	0.0030	0.163
0.9	0.0008	0.110

Table 6.1: Minimum computed axial velocity vs. ϕ for $\alpha = 1$

To obtain an explanation for this phenomenon, the minimum axis velocity was plotted against the swirl parameter K for different values of retardation ϕ as the flow was being driven to stagnation. It can be seen from Fig. 6.5 below that for low values of deceleration ϕ (or conversely for large values of K_{crit}) the curves become steeper as K increases when the axis velocity is not yet close to zero, and apparently small increments in swirl will drive the flow beyond stagnation and into regimes where a solution no longer exists. For larger values of ϕ, or lower values of K_{crit}, the curves eventually become steep but only when the minimum axis velocity is very near zero. Thus, stagnation conditions where best modeled for cases with strong decelerations.

If other values of the retardation parameter ϕ are considered, the main features of this flow are can be summarized by the following observations:

(1) A strong deceleration near the axis of the vortex is caused by large axial pressure gradients induced by the velocity retardation imposed in the outer boundary. This deceleration is depicted in Figs. 6.2, 6.8 and 6.12 for the three different

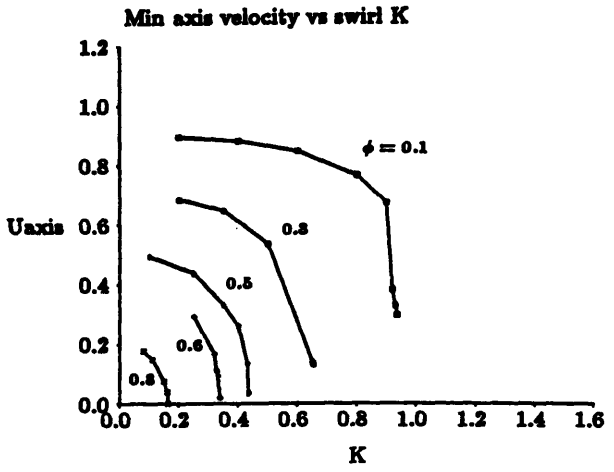

Figure 6.5: Minimum axis velocity vs. swirl K

cases $\phi = 0.1$, $\phi = 0.3$, and $\phi = 0.7$, respectively.

(2) The point of minimum velocity always lies on the vortex axis and at the outflow boundary, as can be seen from Figs. 6.2, 6.8 and 6.12. Both of these results are reasonable, since the axial pressure gradients are strongest at the axis and the total pressure is a minimum, and the deceleration must be felt by the flow up to the exit station. This is because of the elliptic nature of the problem and also because, in the absence of viscosity, no mechanism exists to decelerate the flow other than the imposed outer retardation.

(3) The flow streamlines show that the expansion of the streamtubes is largest at the vortex core region. The core expansion increases with increasing retardation value ϕ. Figs. 6.1, 6.6 and 6.7 show contours of constant streamfunction values, and the above result can be clearly observed for three different cases. The radius of the expanded core is denoted by b, and for stagnation cases b_{crit}.

(4) The deceleration of the flow is more pronounced in the core region for the whole domain, but the patterns are different for the flows before and after the retardation region. Before the retardation is applied at the outer boundary, the maximum axial velocity at a given axial station occurs at the outer boundary itself;

after the retardation has been imposed, this maximum occurs at the vortex core edge. As the flow approaches the exit station, the axial velocity in the outer potential region becomes essentially uniform and equal to $1 - \phi$, with no clearly defined maximum there.

(5) As stagnation is approached the slope of the circumferential velocity profile near the vortex axis becomes very steep, indicating that at stagnation $\frac{\partial w}{\partial \sigma} = 0$ at the axis. This can be observed in Figs. 6.3, 6.9 and 6.13 below. Notice that cases with low retardation ϕ do not show as steep a profile as cases with large velocity retardation. This is due to the fact that only those computations with larger values of ϕ converged at near-stagnation conditions, as explained above.

Notice that the circumferential velocity profile remains unchanged for the outer potential region of the flow, possibly to maintain the value of the circulation constant, as can be expected from Helmholtz's theorem. The maximum circumferential velocity has now decreased to satisfy conservation of angular momentum.

(6) The variation of static pressure with radial distance σ can be seen in Figs. 6.4, 6.10 and 6.14 for different retardation cases. The leftmost curve corresponds to x=0, whereas the rightmost curve corresponds to the exit station x=L. The pressure defect at the inflow boundary increases with swirl K, as can be expected from the radial equilibrium relationship

$$\frac{\partial \overline{p}}{\partial \overline{\sigma}} = K^2 \overline{\sigma}. \tag{6.1}$$

It can be seen that the flow starts with a lower static pressure near the axis, but the pressure starts to rise in the core ahead of the location where the external pressure gradient is imposed. That is, the core pressure rise leads the external pressure rise. Going through the deceleration, the pressure maximum occurs outside the core edge for cases where $\phi \geq 0.3$. Downstream of the region where the deceleration is imposed, the pressure rise in the core of the vortex lags the pressure rise imposed at the outer boundary. Also, an axial pressure gradient develops as a consequence

of the curvature of the streamlines, as the flow expands and even exits the domain through the upper boundary. This pressure gradient is set up independently of the radial gradient that exists due to the rotation of the flow around the vortex axis. The pressure tends to become smoothly uniform with respect to σ as the exit nears for cases with strong decelerations ($\phi \geq 0.6$), as can be seen in Fig. 6.14. At the outflow the streamlines become parallel near the exit, so that the above pressure gradient disappears. For cases with less severe decelerations ($\phi \leq 0.5$) the curvature of the streamlines is not large enough to induce a sufficiently strong pressure gradient that could retard the outer portion of the flow. Thus, the pressure does not become as uniform as for the strong retardation cases (see Figs. 6.4 and 6.10). The results seem to indicate that the stronger the deceleration, the stronger the deviation of the outflow pressure field with respect to the inlet pressure field, favoring uniformity in the vertical direction.

Also notice that for the low retardation cases ($\phi < 0.5$) the pressure values just below the vortex core edge tend to remain fairly constant, the curves coalescing around that region.

(7) It was found that the K_{crit} values found in the numerical study were different from those obtained using the analytical solution of Batchelor [12] (critical conditions meaning stagnation on the axis for Batchelor's solution, lack of convergence for our computation). A comparison of the two sets of values is shown below in Table 6.2 for different values of ϕ. It can be seen that the computational values are higher than the analytical values by as much as 19% for $\phi = 0.1$, descending to around 11% for higher values of retardation. Although the difference in value for $\phi = 0.9$ jumps to close to 53%, no explanation could be found for this behavior. Numerically, it was found that in the absence of external deceleration ($\phi = 0.0$) the flow could not be driven to stagnation for any value of swirl K, as indicated by the ∞ symbol in Table 6.2. However, Batchelor's analytic solution is also satisfied by finite values of swirl K for the case of zero retardation ($\phi = 0.0$), as well as by K= ∞. This is due

to the fact that the solution is double-valued in this limit. Careful consideration of both values reveals that K= ∞ is the proper solution, agreeing with the numerical results.

The computed and analytical values for the core expansion b_{crit} at the outflow station are also given in Table 6.2. Notice again the disagreement between the two sets of values, indicating that although the numerical solution allows a higher K_{crit}, the analytical solution predicts a larger expansion of the vortex core. This difference in the value of b is about 13% for $\phi = 0.1$ and decreases down to about 1.1% for $\phi = 0.7$, so core expansion values tend to agree as the deceleration increases. Observe in Table 6.2 that no b values are given for $\phi = 0.8, 0.9$ since the core expanded beyond the computational domain boundaries.

ϕ	K(analytical)$_{crit}$	K(numerical)$_{crit}$	b(analytical)$_{crit}$	b(numerical)$_{crit}$
0.0	∞	∞	1.000	1.000
0.1	0.786	0.936	1.410	1.223
0.2	0.677	0.779	1.510	1.341
0.3	0.575	0.652	1.627	1.441
0.4	0.480	0.538	1.770	1.582
0.5	0.390	0.434	1.949	1.818
0.6	0.305	0.339	2.190	2.064
0.7	0.224	0.249	2.454	2.427
0.8	0.146	0.163	3.129	$\sim$
0.9	0.072	0.110	4.464	$\sim$
1.0	0.0	0.0	$\sim$	$\sim$

Table 6.2: Comparison of numerical vs analytical values of K_{crit} and b_{crit}

It could be argued that the disagreement in the computed and analytical values is caused by the fact that the solution given by Batchelor assumes that the outflow has constant axial velocity at the potential region outside the vortex core, whereas the computed solution exhibits a slightly nonuniform profile in that region. However, this is likely to be only a minor source of disagreement, the nonuniformity being at worst about 1.2% of the outer boundary value. It is more reasonable to argue that the inaccuracy is caused by the inability to reach stagnation conditions, and by numerical errors.

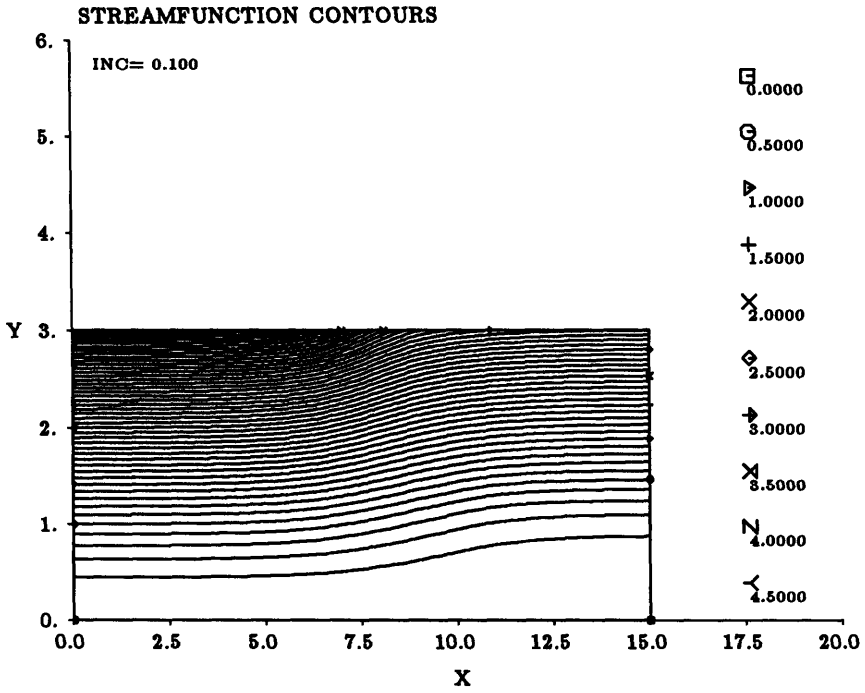

Figure 6.6: Streamfunction, Critical case:$\phi = 0.3, \alpha = 1.0, K = 0.652$

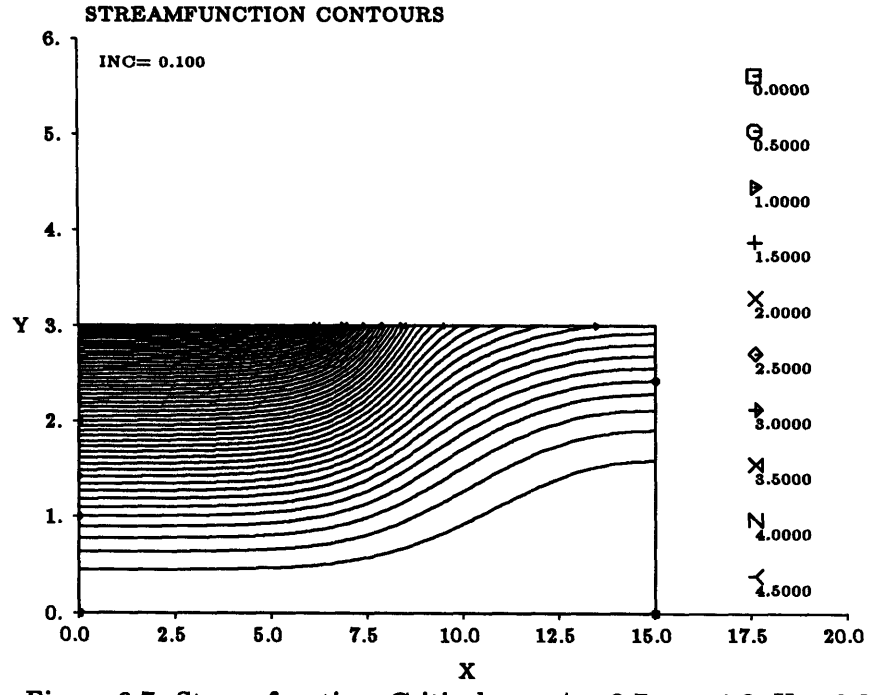

Figure 6.7: Streamfunction, Critical case:$\phi = 0.7, \alpha = 1.0, K = 0.249$

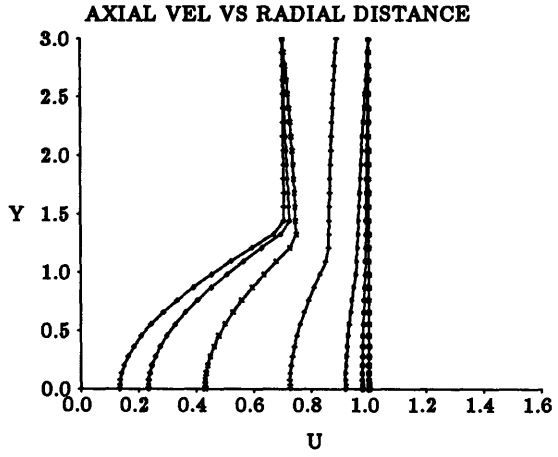

Figure 6.8: Axial Profiles, Critical case:$\phi = 0.3, \alpha = 1.0, K = 0.652$

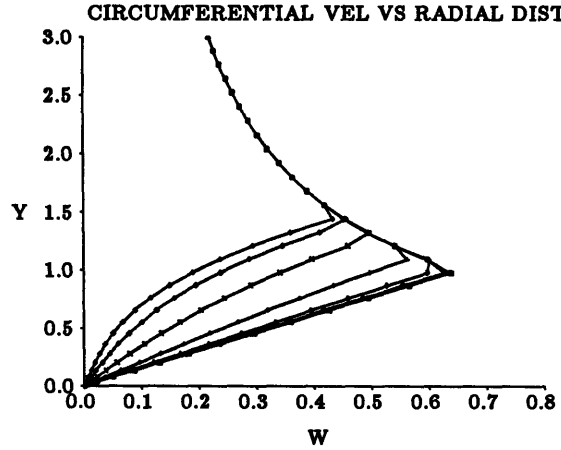

Figure 6.9: Circumf. profiles, Critical case:$\phi = 0.3, \alpha = 1.0, K = 0.652$

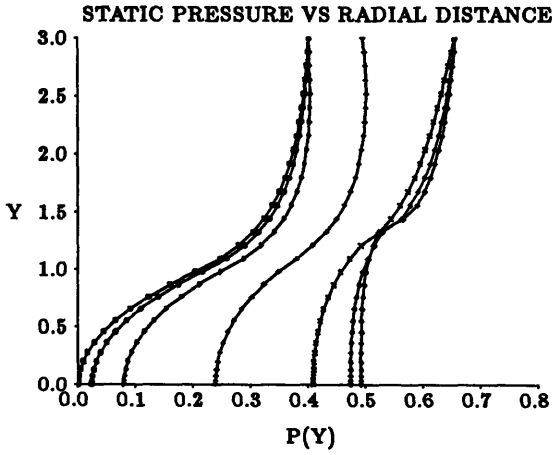

Figure 6.10: Static pressure, Critical case:$\phi = 0.3, \alpha = 1.0, K = 0.652$

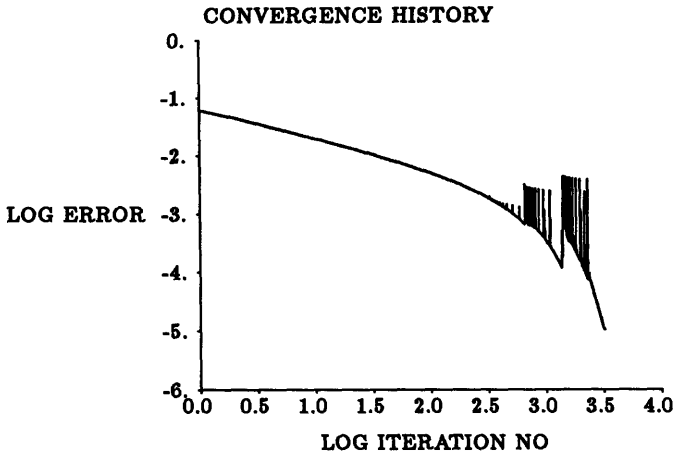

Figure 6.11: Convergence History, Critical case:$\phi = 0.3, \alpha = 1.0, K = 0.652$

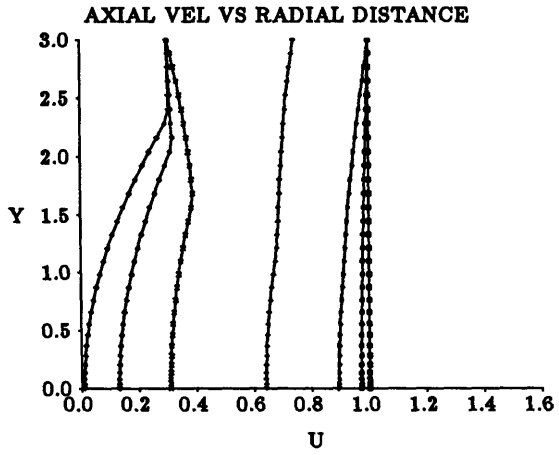

Figure 6.12: Axial Profiles, Critical case:$\phi = 0.7, \alpha = 1.0, K = 0.249$

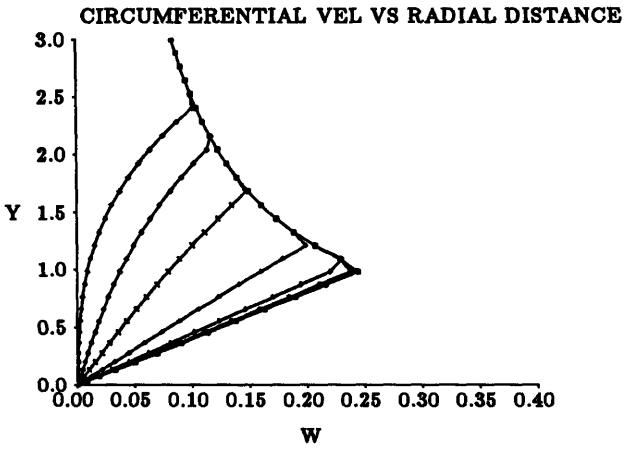

Figure 6.13: Circumf. Profiles, Critical case:$\phi = 0.7, \alpha = 1.0, K = 0.249$

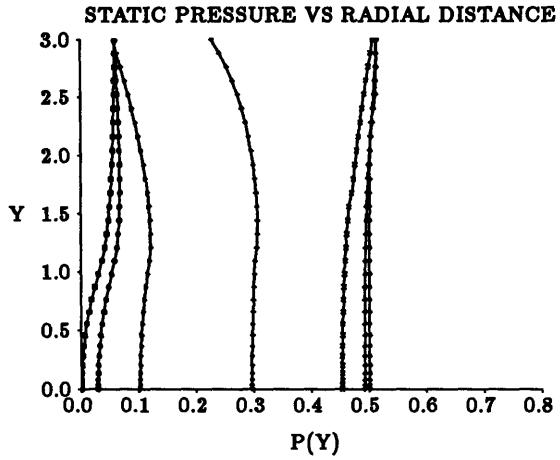

Figure 6.14: Static pressure, Critical case:$\phi = 0.7, \alpha = 1.0, K = 0.249$

6.2 Case II: $\alpha > 1$

An inflow profile parameter $\alpha = 1.2$ was used, and the computation proceeded as in Case I. Both types of flows presented similarities in their behavior, generally with minor differences except for the important fact that $\alpha = 1.2$ flows developed their minimum velocity not at the axis, but at some vertical location within the expanding core region. No analytical solutions are available for comparison with numerical results in this case.

Consider the solution for $\phi = 0.1$, shown in Figs. 6.15, 6.16, 6.17, and 6.18. As for $\alpha = 1.0$, plots of streamfunction, axial and circumferential profiles, and static pressure are given. We see from Fig. 6.15 that the retardation results in a core expansion similar to those observed in $\alpha = 1$ cases. The circumferential velocity shows a decrease in peak value as the core edge moves radially outward, and a change in the slope of the profile within the core. Fig. 6.18 again shows that a large pressure gradient develops at and near the axis. Fig. 6.16 indicates that the minimum axial velocity occurs around $\sigma = 0.5$, and not at the axis. It also shows that this minimum velocity is not zero. Computations with a larger swirl failed to converge.

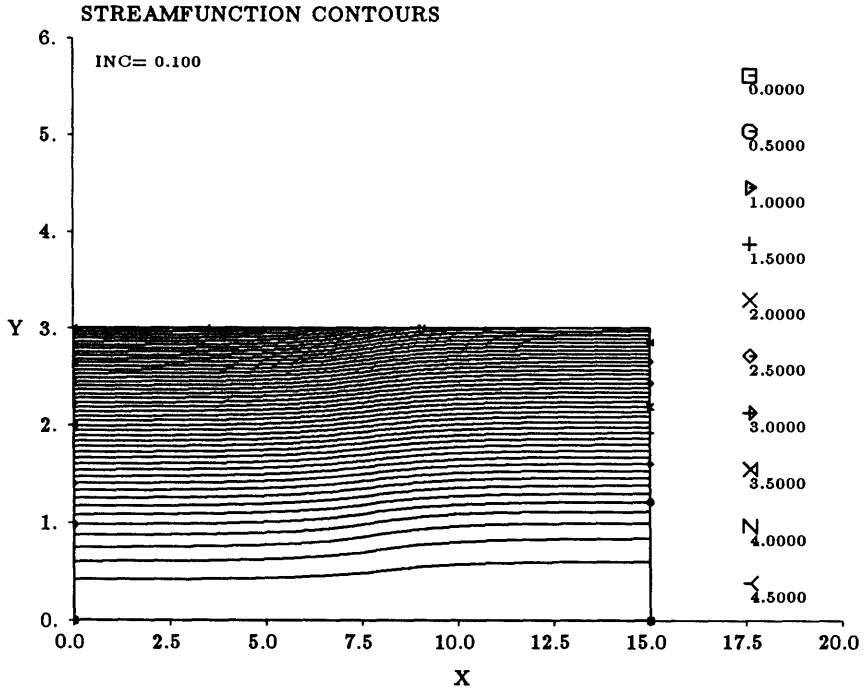

Figure 6.15: Streamfunction, Critical case:$\phi = 0.1, \alpha = 1.2, K = 1.087$

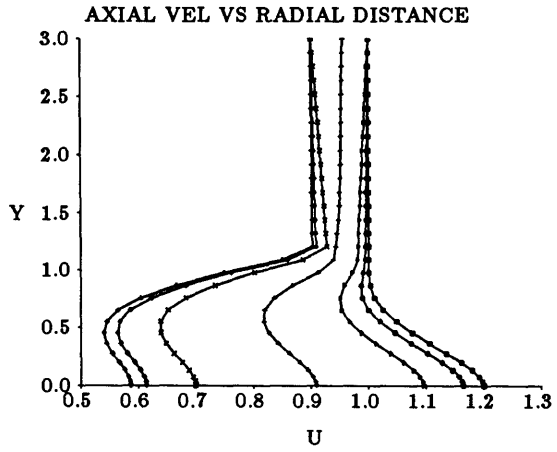

Figure 6.16: Axial Profiles, Critical case:$\phi = 0.1, \alpha = 1.2, K = 1.087$

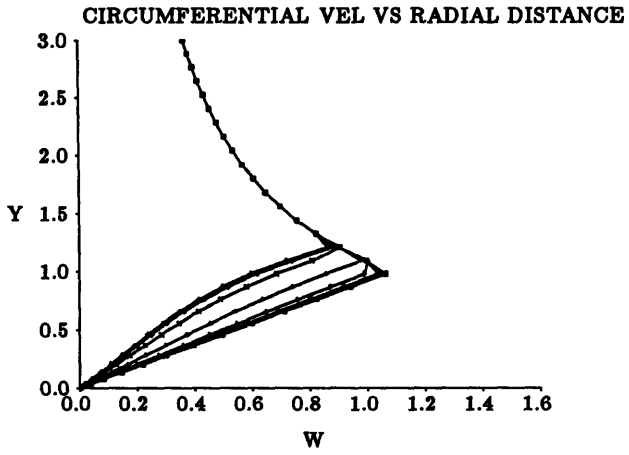

Figure 6.17: Circumf. Profiles, Critical case:$\phi = 0.1, \alpha = 1.2, K = 1.087$

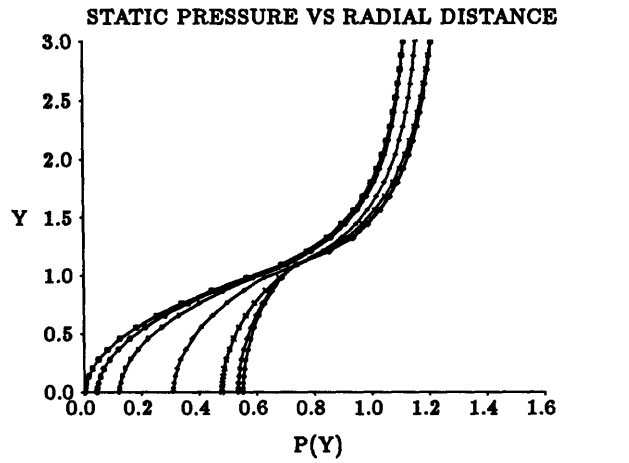

Figure 6.18: Static pressure, Critical case:$\phi = 0.1, \alpha = 1.2, K = 1.087$

Therefore, the computations failed again to converge for some value of swirl K as the flow approached stagnation conditions. As expected, having a jet-like inlet axial profile delayed the onset of stagnation as compared with the uniform axial profile cases (for the same retardation value ϕ). Thus, the swirl parameter K had to be highly increased beyond the values given by the $\alpha = 1$ solution. This can be observed in Table 6.3 below, where the minimum exit axial velocities are presented for retardation values of $\phi = 0.1, 0.3, 0.5$, together with the critical swirl parameter

value and the location of the minimum Y_{min}. The axis velocity at the exit is also presented for comparison.

ϕ	K_{crit}	$U_{minimum}$	U_{axis}	Y_{min}
0.1	1.087	0.538	0.584	0.454
0.3	0.819	0.356	0.481	0.760
0.5	0.619	0.150	0.442	1.090

Table 6.3: Minimum axial, and axis velocity vs. ϕ for $\alpha = 1.2$

It was not possible to obtain meaningful results for retardation values $\phi \geq 0.7$, since the core expanded beyond the boundary limits of the domain, resulting in specified velocities at the outer boundary that had no physical validity.

It can be observed from the streamfunction contour plots in Figs. 6.15 and 6.19 that the expansion of the vortex core now takes place within a smaller axial length as compared with $\alpha = 1$ cases. In this case the streamlines become horizontal more quickly and at a larger distance from the exit of the domain. Thus, the outflow boundary condition $\frac{\partial \Psi}{\partial x} = 0$ is met more naturally in this type of flow. Careful observations of the contour plots reveal that the streamtube expansion is not largest in the region nearest the axis, but rather in a concentric region located about half a core in the radial direction, indicating that the axial pressure gradient becomes largest there. This is probably a consequence of the curvature of the streamlines being largest in this region, an indication that the flow nearest the axis can now negotiate the adverse pressure gradient better than the fluid surrounding it, possibly due to a higher total head value.

In fact, the axial velocity plots in Figs. 6.16 and 6.20 show that the minimum axial velocity does not occur at the axis anymore, but somewhere within the vortex

core at the exit station. Therefore, stagnation of the flow might not lead in this case to a bubble sitting on the axis but rather to an annulus filled with recirculating fluid surrounding a forward moving jet at the axis.

It is interesting to note that experimental observations of the internal structure of the bubble by Faler and Leibovitch [9] reveal that the latter consists of two cells or annuli of recirculating fluid, with the smaller cell embedded inside the larger one. The experimental results show that the flow develops a stagnation point at the axis where the bubble is first encountered, although other stagnation points can be found inside the structure. Although the numerical solution could at most predict a stagnant ring around the vortex axis (leaving unanswered the question of how this ring could develop into the two-celled structure that is observed experimentally), the possibility exists that once backflow sets in, this upstream moving mass of fluid eventually turns to flow downstream. This pattern could immediately set up a stagnation point at the axis from where the bubble would develop, the recirculating annuli now part of its inner structure. Notice also that the approach flow used in the experiments performed by several researchers who obtained vortex bursting, including Faler and Leibovitch, exhibited a jet profile [3,4,5,9,13,14,15,16], and the same jetlike axial motion was measured by Singh and Uberoi[17] in trailing vortices near wing tips. Hence, it is possible that flows with jet profiles could model the inner structure of a bursting bubble better than the uniform inlet profiles.

It can be observed from the circumferential velocity plots (Figs. 6.17 and 6.21) that the effect of the axial retardation on the circumferential profile is to slow down the rotation in the annular region between the vortex axis and the core edge. As the retardation parameter ϕ increases, this behavior becomes exagerated, affecting mostly the outer core region (Fig. 6.21).

The static pressure plots shown in Figs. 6.18 and 6.22 reveal a behavior similar to the one observed in $\alpha = 1$ cases up to the point where the core starts to expand.

It can be seen that the pressure curve develops a kink at the exit, possibly due to the rapidly varying circumferential velocity and the need to balance the centripetal force there.

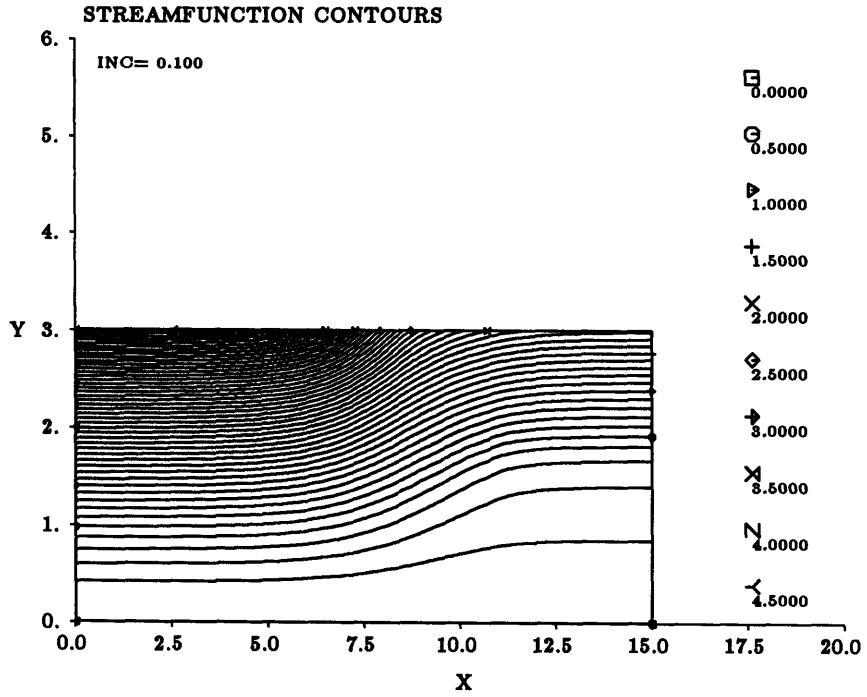

Figure 6.19: Streamfunction, Critical case:$\phi = 0.5, \alpha = 1.2, K = 0.619$

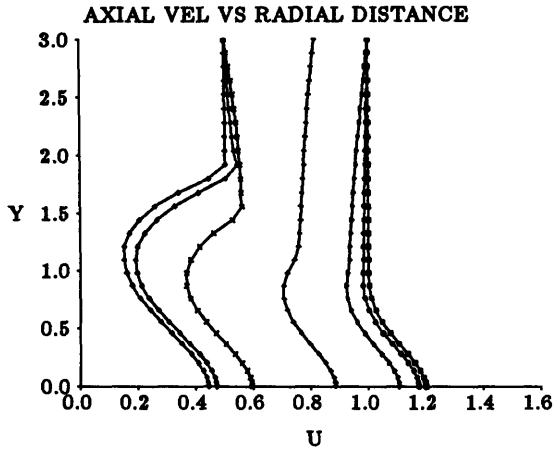

Figure 6.20: Axial Profiles, Critical case:$\phi = 0.5, \alpha = 1.2, K = 0.619$

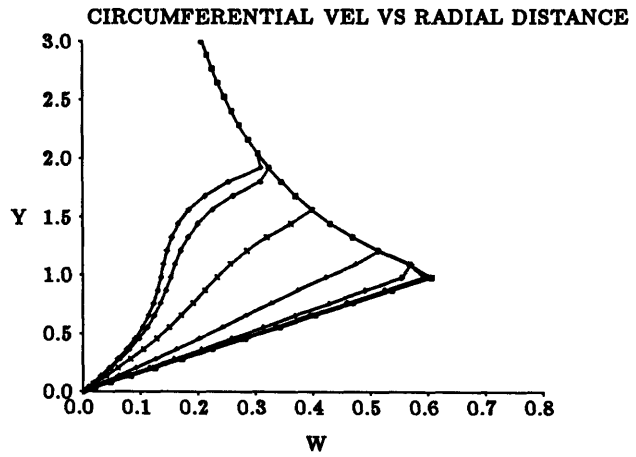

Figure 6.21: Circumf. Profiles, Critical case:$\phi = 0.5, \alpha = 1.2, K = 0.619$

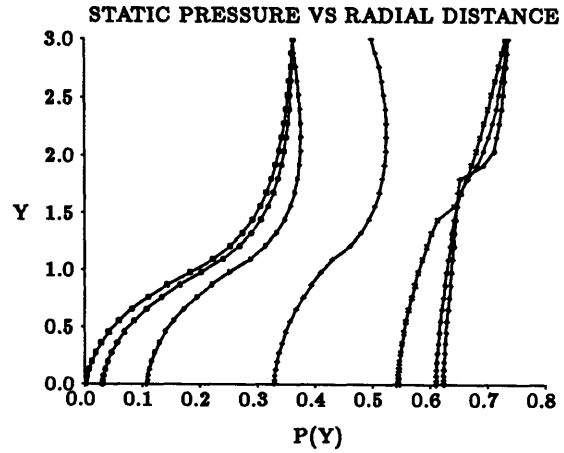

Figure 6.22: Static Pressure, Critical case:$\phi = 0.5, \alpha = 1.2, K = 0.619$

6.3 Case III: $\alpha < 1$

A profile parameter $\alpha = 0.8$ was chosen for this case. This type of flow showed less variations with respect to $\alpha = 1.0$ cases than $\alpha = 1.2$ cases. It was found that the swirl required to drive a flow to stagnation was less than that for uniform inlet profile cases. However, the flow behavior was essentially similar to the one considered in Case I and no new major features were observed. Thus, the minimum axial velocity occurred on the axis and at the outflow station. Again, no converged solution was obtained for which the flow showed stagnation conditions, although for $\phi \geq 0.3$ the minimum axial velocity was very close to zero.

Figs. 6.23, 6.24, 6.25, and 6.26 below show results for the case given by $\phi = 0.3$. Typical streamline, axial velocity, circumferential velocity, and static pressure plots are presented. Comparing the axial velocities with those for $\alpha = 1.0$ cases, it can be seen from Fig. 6.24 that the flow can now be driven to stagnation with lower values of swirl parameter K for the same value of retardation ϕ. In fact, it was very difficult to obtain any converged solution for $\phi > 0.3$ for which the axis velocity approached zero.

Notice from Fig. 6.23 that the core expansion characteristics are similar to those presented for $\alpha = 1.0$ cases. However, Fig. 6.25 shows that the steepening and curving of the circumferential profile is now confined to the region of the core nearest the vortex axis, the outer core region still showing a rigid body rotation profile. The static pressure plot presented in Fig. 6.26 is not very different from pressure plots for $\alpha = 1.0$ cases.

The critical values of swirl K are presented below in Table 6.4 for three different values of retardation ϕ, together with the minimum axis velocity.

ϕ	$U_{minimum}$	K_{crit}
0.1	0.428	0.740
0.2	0.178	0.561
0.3	0.008	0.373

Table 6.4: Minimum axial velocity and K vs. ϕ for $\alpha = 0.8$

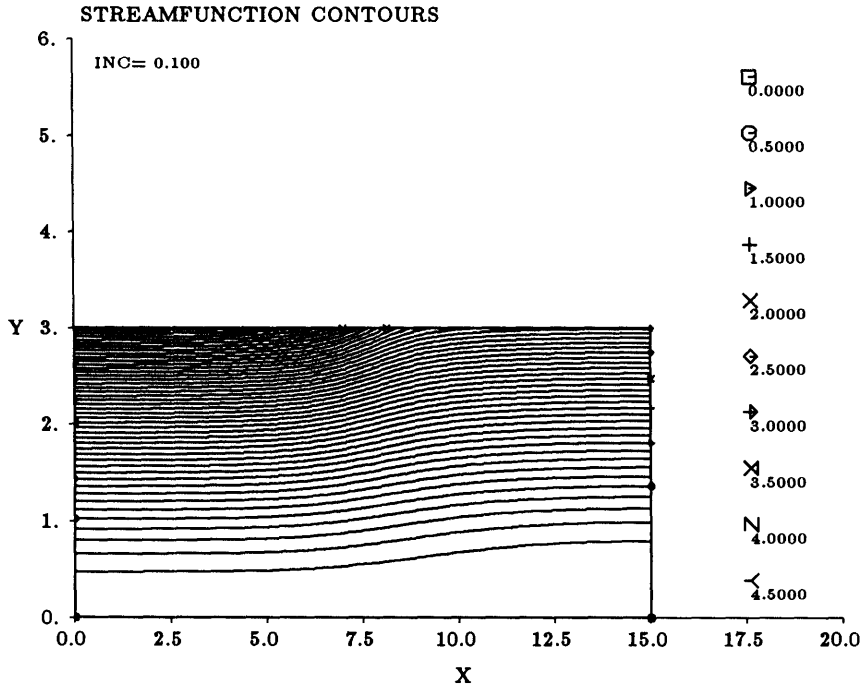

Figure 6.23: Streamfunction, Critical case: $\phi = 0.3, \alpha = 0.8, K = 0.373$

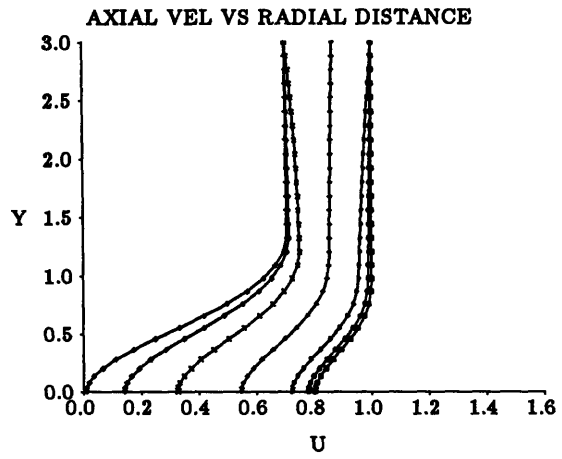

Figure 6.24: Axial Profiles, Critical case: $\phi = 0.3, \alpha = 0.8, K = 0.373$

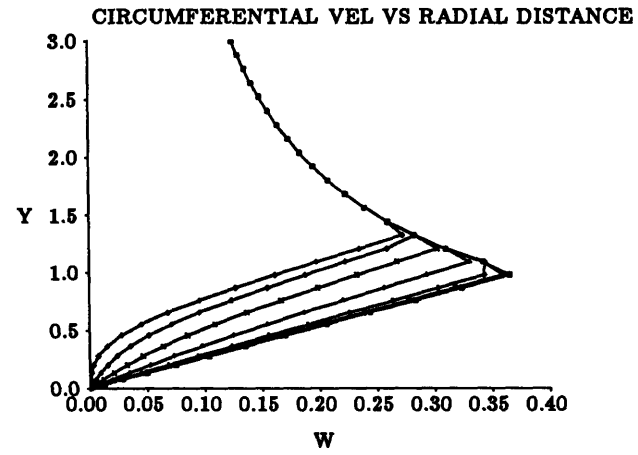

Figure 6.25: Circumf. Profiles, Critical case: $\phi = 0.3, \alpha = 0.8, K = 0.373$

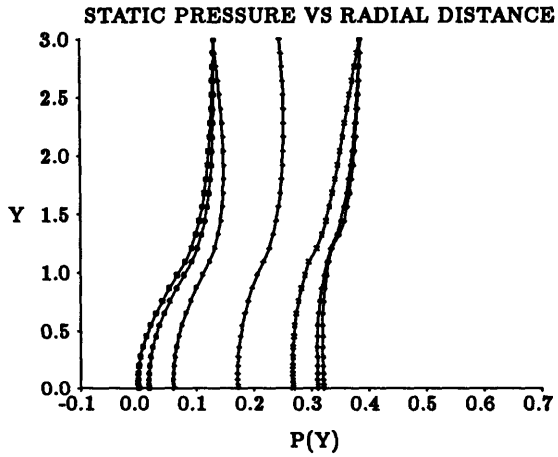

Figure 6.26: Static Pressure, Critical case: $\phi = 0.3, \alpha = 0.8, K = 0.373$

6.4 Case IV: Powell's Input Profile

As mentioned above, Powell derived a self-similar, conical solution to the Navier-Stokes equations that show good agreement with the experimental results of Earnshaw for leading edge vortices of a delta wing [21].

The object of trying the velocity profiles of Powell as upstream boundary conditions in the present inviscid model was to compare the previous results for $\alpha = 1.2$ with results obtained with a more realistic profile.

The input solution used in this study was obtained from Powell's model with a Reynolds number of 100, a circulation value of 0.22, an outer edge radius of 1.55, and an outer edge velocity equal to 1.0. These parameters gave a jet of maximum velocity equal to 1.216 at the axis, a swirl parameter K=0.34, and a domain radius R=3.06 (after normalizing lengths with the core radius defined in section 5.3). This set of parameters was deemed appropriate, since further manipulation of the input values failed to give profiles closer to the $\alpha = 1.2$ case. To make a useful comparison, a computation with the same values for K and R was performed using the standard upstream profile with $\alpha = 1.216$ (see Eqn. 2.5).

Unlike the previous cases, this computation involved increasing the retardation value ϕ, with swirl K fixed, until stagnation or divergence was encountered. The reason for not following the standard procedure is that the swirl parameter K given by Powell's solution is a function of the specified circulation and the Reynolds number. Changing either one of these parameters results in substantial changes in the velocity profile and the normalized domain radius. Therefore, it was easier to keep the swirl constant, increasing the magnitude of the retardation.

The results for the computation using Powell's input profile are shown below in Figs. 6.27, 6.28, 6.29, and 6.30. Those using an $\alpha = 1.216$ profile are shown in Figs. 6.31, 6.32, 6.33, and 6.34. Again, constant streamfunction contour plots, axial

velocity profile, circumferential velocity, and static pressure are given.

Notice that the magnitude of retardation needed to drive the flow to stagnation was slightly different for the two profiles. Whereas for Powell's profile $\phi = 0.71$, for the standard profile with $\alpha = 1.216$ it was $\phi = 0.79$.

Figs. 6.27 and 6.31 show the streamfunction contour plots. Notice that the expansion of the streamtubes is largest near the axis for Powell's case, whereas for $\alpha = 1.216$ it occurs near the edge of the vortex core. Hence, the plots seem to indicate that Powell's profile leads to stagnation on the axis, whereas the $\alpha = 1.216$ profile would lead to the development of a stagnation ring around the axis (see Case II results).

Comparison of Figs. 6.28 and 6.32 show differences in axial velocity profiles. Clearly, Powell's upstream profile suffers the strongest deceleration near the axis, whereas the standard profile tends to stagnate around $\sigma = 2.0$. Further deceleration of this profile was impractical, since the vortex core would have expanded beyond the domain boundaries.

Figs. 6.29 and 6.33 show circumferential velocity profiles. It can be observed that Powell's outer profile does not approach a potential vortex profile, although the boundary condition at the upper radial boundary in his model was specified such that the circumferential velocity would decay as $\frac{1}{\sigma}$. As a result, and in order to conserve angular momentum, the whole circumferential profile suffers a deceleration, in contrast with the $= 1.216$ case, for which the outer profile remains unaltered and only a decrease of maximum circumferential velocity is observed. The steepening of the curves as the outflow boundary is approached can be observed in both plots, although Powell's profile feels this effect near the axis while the standard profile arches near the core edge.

The static pressure curves shown in Figs. 6.30 and 6.34 reveal a similar pattern

appearance, but they differ considerably in real value. Notice that Powell's curves start with negative values at the inflow boundary (local pressure is lower than at upstream infinity) whereas the standard profile assumes zero difference in pressure at the inflow with respect to upstream infinity (at the axis).

These results seem to indicate that the phenomenon strongly depends on the choice of upstream boundary conditions. Since the axial velocity profiles were similar in form and in magnitude, it can be argued that the difference in circumferential velocity profiles and in static pressure values upstream are mainly responsible for the disagreement between the two cases considered.

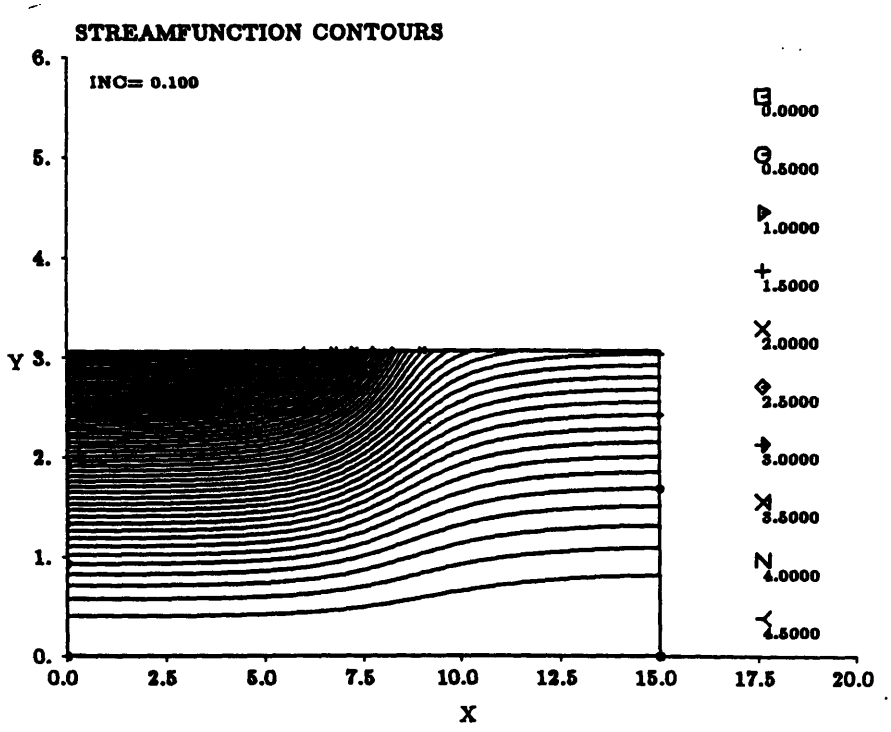

Figure 6.27: Streamfunction, Critical case: $\phi = 0.71$, Powell profile, $K = 0.34$

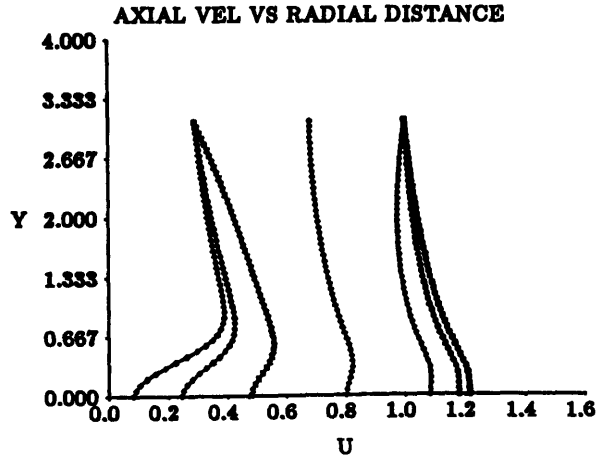

Figure 6.28: Axial Profiles, Critical case: $\phi = 0.71$, Powell profile, $K = 0.34$

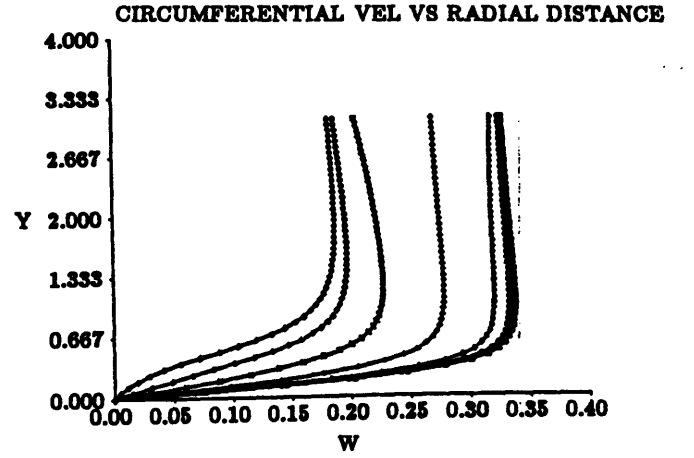

Figure 6.29: Circumf. Profiles, Critical case: $\phi = 0.71$, Powell profile, $K = 0.34$

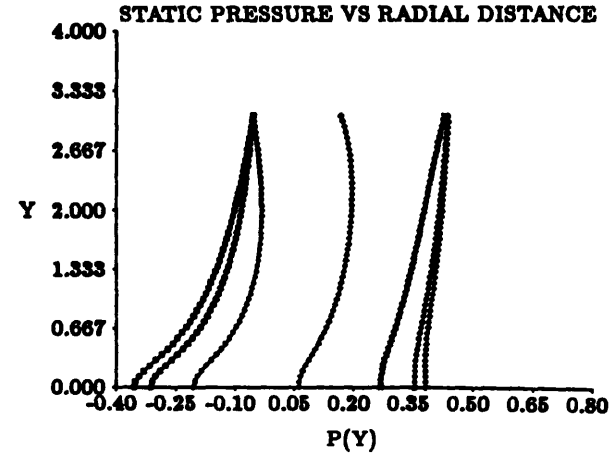

Figure 6.30: Static Pressure, Critical case: $\phi = 0.71$, Powell profile, $K = 0.34$

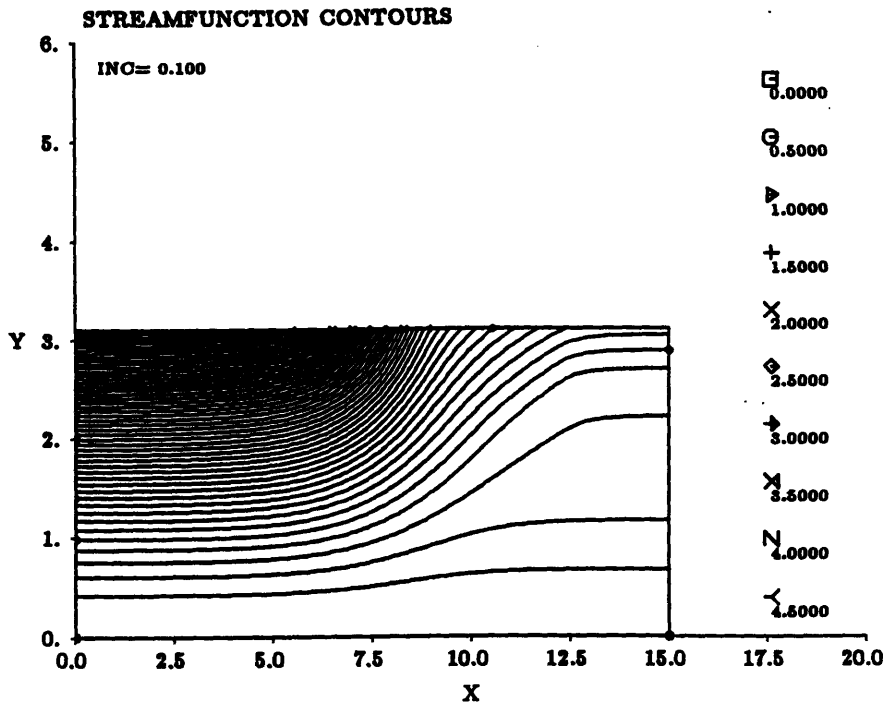

Figure 6.31: Streamfunction, Critical case: $\phi = 0.79, \alpha = 1.216, K = 0.34$

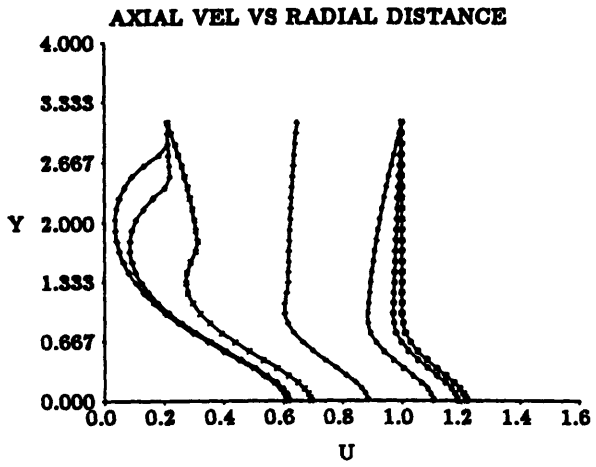

Figure 6.32: Axial Profiles, Critical case: $\phi = 0.79, \alpha = 1.216, K = 0.34$

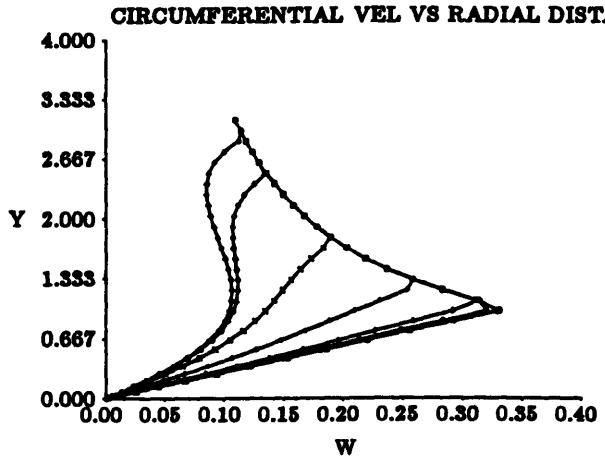

Figure 6.33: Circumf. Profiles, Critical case: $\phi = 0.79, \alpha = 1.216, K = 0.34$

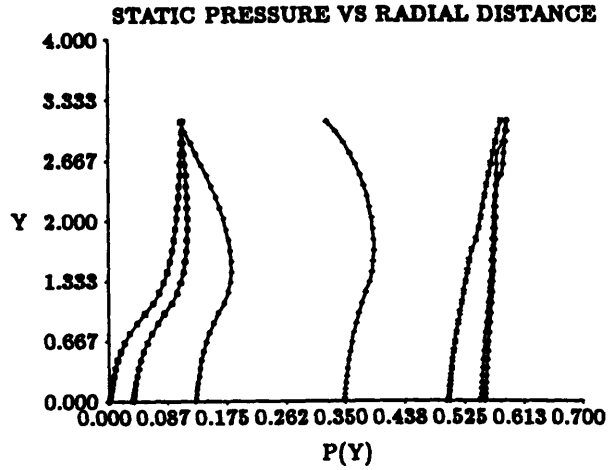

Figure 6.34: Static Pressure, Critical case: $\phi = 0.79, \alpha = 1.216, K = 0.34$

Chapter 7
Conclusion

The phenomena associated with the deceleration of a free axisymmetric vortex by a pressure gradient at the outer boundary has been numerically studied using an inviscid scheme. By considering relevant physical parameters it was possible to vary the flow conditions and assess the relative importance of each one of the factors, and their combination.

A set of numerical data has been obtained to serve as a test of comparison with other computational results that may appear in the future, viscous and inviscid. These results were compared with analytical solutions by Batchelor [12], showing good agreement for general non-critical cases. The agreement was not as good though, for prediction of critical values of swirl and core expansion.

No conclusive evidence was found that vortex bursting is caused by an inviscid mechanism, but the results hint at the possibility that the onset of bursting is an inviscid phenomenon. Values of axis velocity close to zero for uniform inlet profile flows indicate that stagnation is possible without resorting to viscosity, and only numerical discretization errors are believed to be responsible for preventing a solution with zero total velocity. The behavior exhibited by the flow was similar to the one observed in vortex bursting experiments, especially regarding velocity profiles and pressure fields.

Of great interest are the results for jet-like inlet profile flows, showing that perhaps they model the mechanism of bursting more faithfully than uniform inlet flows. Following this line of thought, the self-similar solution to the conical Navier-

Stokes equations of Powell [11] were used as upstream boundary conditions to study the characteristics of the deceleration on realistic profiles.

It was found that these characteristics depend strongly on the choice of upstream boundary conditions. Some profiles develop stagnation at the axis, while others develop stagnation rings around the axis. It would be interesting to perform physical experiments to assess the correctness of the numerical results, and whether or not the two types of stagnation lead to the same phenomena.

Bibliography

[1] Landahl, M. T. and Widnall, S. E. : *Vortex Control*, Aircraft Wake Turbulence and its Detection, Plenum Press, New York (1970).

[2] Peckham, D. H. and Atkinson, S. A. : *Preliminary results of low wind tunnel tests on a gothic wing of aspect ratio 1*, Aero. Res. Counc. CP no. 508, 1957.

[3] Sarpkaya, T. : *On Stationary and Traveling Vortex Breakdowns*, J. Fluid Mech., 1971, vol.75, pp 545-559.

[4] Sarpkaya, T. : *Vortex Breakdown in Swirling Conical Flows*, AIAA Journal, 1971, vol.9, pp.1792-1799.

[5] Lambourne, N. C. and Bryer, D. W. : *The Bursting of Leading-Edge Vortices - Some Observations and Discussion of the Phenomenon*, Aero. Res. Counc. Reports and Memoranda No. 3282, April 1961.

[6] Payne, F. M., Ng, T. T. and Nelson, R. C. : *Visualization and Flow Surveys of the Leading Edge Vortex Structure on Delta Wing Planforms*, AIAA-86-0330.

[7] Hafez, M. M. and Salas, M. D. : *Vortex Breakdown Simulation Based on a Nonlinear Inviscid Model*, Studies of Vortex Dominated Flows, Springer-Verlag, 1987.

[8] Leibovich, S. : *The Structure of Vortex Breakdown*, Ann. Rev. of Fluid Mechanics, 1978, vol.10, pp. 221-246.

[9] Faler, J. H. and Leibovich, S. : *An experimental map of the internal structure of a vortex breakdown*, J. Fluid Mech., 1977, vol. 86, Part 2, pp. 313-335.

[10] Grabowski, W., and Berger, S. : *Solutions of the Navier-Stokes equations for vortex breakdown*, J. Fluid Mech., 1976, vol.75, pp. 525-544.

[11] Powell, K. G. : *Vortical Solutions of the Conical Euler Equations*, PhD Thesis, CFDL, Massachusetts Institute of Technology, July 1987.

[12] Batchelor, G. K. : An Introduction to Fluid Dynamics, Cambridge University Press, 1967, pp. 543-555.

[13] Pagan, D. and Benay, R. : *Vortex breakdown induced by an adverse pressure gradient: experimental and numerical approaches*, AIAA Journal, 1987.

[14] Harvey, J. K. : *Some Observations of the Vortex Breakdown Phenomenon*, J. Fluid Mech., 1962, vol. 14, pp. 585-592.

[15] Kirkpatrick, D. L. I. : *Experimental investigation of the breakdown of a vortex in a tube*, Aero. Res. Counc. CP 821, 1964, pp. 9-18.

[16] Garg, A. K. : *Oscillatory behavior in vortex breakdown flows: an experimental study using a laser doppler anemometer*, MS thesis, Cornell University, 1977.

[17] Singh, P. I. and Uberoi, M. S. : *Experiments on vortex stability*, Physics of Fluids, 1976, vol. 19, pp. 1858-1863.

[18] Benjamin, B. : *Theory of the vortex breakdown phenomenon*, J. Fluid Mech., 1962, vol.14, pp. 593-629.

[19] Benjamin, B. : *Some developments in the theory of vortex breakdown*, J. Fluid Mech., 1967, vol.28, pp. 65-84.

[20] Hall, M. G. : *Vortex Breakdown*, Ann. Rev. of Fluid Mechanics, 1972, vol.10, pp. 195-218.

[21] Earnshaw, P. B. : *An Experimental Investigation of the Structure of a Leading-Edge Vortex*, Reports and Memoranda 3281, Aeronautical Research Council, 1961.

```
C       INCLUDE FILE 'NEWVRTXCOM.INC' FOR BATCHVRTX1.FOR PROGRAM
C
        IMPLICIT REAL (A-H,O-Z)
        PARAMETER (NX=200,NY=200)
        COMMON /C0100/ PSI(NX,NY),PSIOLD(NX,NY)
        COMMON /C0200/ PSII(NY),H(NY),DH(NY),CIR(NY)
        COMMON /C0300/ DC(NY),X(NX),Y(NY),Z(NY)
        COMMON /C0400/ XX(NX,NY),YY(NX,NY),YGEN(5*NY)
        COMMON /C0500/ AA(NX),BB(NX),CC(NX),DD(NX)
        COMMON /C0600/ CX(NX),DCC(NX),DHH(NX)
        COMMON /C0700/ U(NX,NY),V(NX,NY),W(NX,NY)
        COMMON /C0750/ PINFLX(NX,NY),VORT(NX,NY)
        COMMON /C0770/ PINFLX1(2.*NY),YNFLX(2.*NY)
        COMMON /C0775/ EPS(4001),STM(4001),NIP(1)
        COMMON /C0776/ IERROR(NX),JERROR(NY)
        COMMON /C0780/ CIRCLN(NX,NY),TOTHEAD(NX,NY),TOTVEL(NX,NY)
        COMMON /C0790/ AXI(NY),TOTPRESS(NY)
        COMMON /C0800/ ALPHA,BETA,PHI,PI,OMEGA,EPSILON,XRET
        COMMON /C0900/ XK,DELTAX,DELTAY,SL,XL,RD,NXP,NYP,XKY,XKB,XB
        COMMON /C1000/ R,RR,RRR,BX,NNN,MP,IGOR,JN,IL,IU,VL,XKSTAG
        COMMON /C1010/ AX,D1,D2,D3,JCORE,DJ,TH1,TH2,RS1,RS2,MMP
        COMMON /C1015/ UMINO,XBSTAG
        COMMON /C1020/ IOPT(1),NPOINTS(1),NNPP(1),NLINE(2)
        COMMON /C1025/ JOPT(2),NNPP2(2),LOPT(1)
        COMMON /C1030/ UBOUND(NX),UINIT(NY),BETAX(NY)
        COMMON /C1040/ UMID2(NY),UMID4(NY),UMID34(NY),UEND(NY)
        COMMON /C1045/ UMID38(NY),UMID58(NY)
        COMMON /C1050/ UO(NX),UO2(NX),VTOP(NX),UTOP(NX),UBESS(NY)
        COMMON /C1053/ VTOP2(NX),VAXIS(NX),U2(NY),U3(NY),WBESS(NY)
        COMMON /C1055/ WINIT(NY),WMID4(NY),WMID2(NY),WEND(NY)
        COMMON /C1056/ WMID38(NY),WMID58(NY),WMID34(NY)
        COMMON /C1057/ PRESSR(NX,NY),PRS(7*NY),UGEN(7*NY)
        COMMON /C1058/ NR(7),KOPT(7),WGEN(7*NY)
        COMMON /C1060/ INDGR,MPT,NPT,THETA1,THETA2,ETA1,ETA2
        COMMON /C1070/ UCONT1,UCONT2,VCONT,UMASS,JCOREB,WEJ1
        COMMON /C1080/ UCONT3,UCONT4,VCONT2,VCONT4,UMASS2,UMASS3
        COMMON /C1090/ UCONT5,VCONT5,UMASS5,BEJO,BEJ1,II
        COMMON /C1095/ UCONT6,UCONT7,VCONT6,VCONT7,UMASS6
        COMMON /C1100/ XY,XXX,YX,YYY,JVORT(6),IVORT(6),XVORT(6)
        COMMON /C1150/ YVORT(6)
        DIMENSION CONT(50)
        CHARACTER*60 TITLE,PLTITL1,PLTITL2,PLTITL3,PLTITL4,PLTITL5
        CHARACTER*60 PLTITL6,PPTLL20,PPTLL21,PPTLL30,PPTLL18,PPT
        CHARACTER*60 PPTLL,PPTLL2,PPTLL3,PPTLL4,PPTLL5,PPTLL10
        CHARACTER*60 PLTITL7,PLTITL8,PLTITL9,PPTLL11,PPTLL40
        CHARACTER*60 PPTLL12,PPTLL13,PPTLL14,PPTLL15,PLTITLGRD
        CHARACTER*60 PPTLL48,PPTLL49,PPTLL50,PPTLL47
        CHARACTER*60 SUBTITLE,SUBPLTITL,PPTLL60,PPTLL61
        TITLE='SIMULATION OF VORTEX BURSTING: NO WALLS'
        SUBTITLE='KB VALUES OF STAGNATION'
        SUBPLTITL='~FUNCTION~PHI=0.1'
        PLTITL1='X~Y~STREAMFUNCTION CONTOURS'
```

```
PPT='X~Y~GRID'
PLTITL2='X~Y~VELOCITY VECTOR'
PLTITL3='X~Y~AXIAL VELOCITY CONTOURS'
PLTITL4='X~Y~TOTAL VELOCITY CONTOURS'
PLTITL5='X~Y~PRESSURE CONTOURS'
PLTITL6='X~Y~CIRCULATION CONTOURS'
PLTITL7='X~Y~TOTAL PRESSURE CONTOURS'
PPTLL='X~UO~AXIAL VELOCITY ON AXIS'
PPTLL2='X~UOUT~AXIAL VELOCITY AT UPPER EDGE'
PPTLL3='X~U~AXIAL VELOCITY AT L/4'
PPTLL4='X~U~AXIAL VELOCITY AT L/2'
PPTLL5='X~U~AXIAL VELOCITY AT 3L/4'
PPTLL10='X~VTOP~RADIAL VELOCITY AT UPPER EDGE'
PPTLL11='X~UTOP~EXACT AXIAL VEL AT UPPER EDGE'
PPTLL12='W~Y~INLET CIRCUMFERENTIAL VELOCITY'
PPTLL13='W~Y~CIRCUMFERENTIAL VELOCITY AT L/4'
PPTLL14='W~Y~CIRCUMFERENTIAL VELOCITY AT L/2'
PPTLL15='W~Y~EXIT CIRCUMFERENTIAL VELOCITY'
PPTLL18='UEXIT~Y~CORE OUTFLOW AXIAL PROFILE'
PPTLL20='HEAD~PSI~INLET HEAD PROFILE'
PPTLL21='CIRCULATION~PSI~INLET CIRCULATION PROFILE'
PPTLL30='PSII~Y~INLET STREAMFUNCTION PROFILE'
PPTLL40='Y~VORTICITY~VORTICITY VS. INFLEXION POINT'
PLTITL8='U~Y~INLET AXIAL VELOCITY'
PLTITL9='U~Y~EXIT AXIAL VELOCITY'
PLTITLGRD='X~Y~GRID PLOT'
PPTLL47='LOG ITERATION NO~LOG ERROR~CONVERGENCE HISTORY'
PPTLL48='U~Y~AXIAL VEL VS RADIAL DISTANCE'
PPTLL49='P(Y)~Y~STATIC PRESSURE VS RADIAL DISTANCE'
PPTLL50='W~Y~CIRCUMFERENTIAL VEL VS RADIAL DISTANCE'
PPTLL60='I~IERROR~AXIAL LOCATION VS ERROR FREQUENCY'
PPTLL61='JERROR~J~VERTICAL LOCATION VS ERROR FREQUENCY'
```

```
      PROGRAM BATCHVRTX1
C
C*************************************************************************
C*************************************************************************
C****   PROGRAM TO SIMULATE THE INVISCID BEHAVIOR  OF A   ****************
C****                    VORTEX NEAR BREAKDOWN            ****************
C*************************************************************************
C*************************************************************************
C
C       REGION NEAR AXIS IS RESOLVED USING LOG FUNCTION.  USES BESSEL
C       FUNCTION FOR ALPHA=1 PROFILES TO COMPARE RESULTS.
C
        INCLUDE 'NEWVRTXCOM.INC'
C
        CALL INPUT
C
        CALL DOMAIN
C
        NNN=1
C
10      CALL UPSTREAM
C
        IGOR=1
C
        CALL SIDES
C
        CALL INITIALIZE
C
        CALL HEAD
C
        CALL CIRCULATION
C
        CALL SPLINE(H,DH,PSII,JCORE)
C
        CALL SPLINE(CIR,DC,PSII,JCORE)
C
        MP=0
18      EPSILON=0.0
C
        DO 25 JN=2,NYP
          CALL COMPUTATION
25      CONTINUE
C
        IF(EPSILON.NE.0.0)THEN
          EPS(MP)=ALOG10(EPSILON)
        ENDIF
        MP=MP+1
        IF(MP.GT.3000.AND.EPSILON.GT.1.0E-02)THEN
           MP=MP-1
           GO TO 300
        ELSEIF(MP.GE.MMP)THEN
           GO TO 300
```

```
        ENDIF
C
        IF(EPSILON.GT.1.0E-05) GO TO 18

 300        CALL VELOCITY
C
C
            CALL PLOT
            STOP
C       ENDIF

        END
C*************************************************************************
        SUBROUTINE INPUT
C*************************************************************************
C       MUST USE INPUT FILE VRTXDATA1.DAT
C
        INCLUDE 'NEWVRTXCOM.INC'

        OPEN(UNIT=10,FILE='VRTXDATA1.DAT',STATUS='OLD')

C.......THE SWIRL PARAMETER K IS K=CORE RADIUS*OMEGA/U(INFINITY)
C.......AND REPRESENTS THE
C.......NONDIMENSIONALIZED CIRCULATION AT THE CORE OF THE VORTEX.
C.......IT IS REPRESENTED BY XK.

        READ(10,*)XK

C.......THE UPSTREAM AXIAL VELOCITY PROFILE IS GIVEN AS A FUNCTION OF THE
C.......RADIAL DISTANCE Y AND OF THE PARAMETER ALPHA. ALPHA LESS THAN 1
C.......GIVES A WAKE-LIKE PROFILE, ALPHA EQUAL TO 1 GIVES UNIFORM AXIAL
C.......FLOW, ALPHA GREATER THAN 1 GIVES A JET-LIKE PROFILE.

        READ(10,*)ALPHA

C.......THE PARAMETER PHI CONTROLS THE ACCELERATION OF THE FLOW AT THE
C.......UPPER BOUNDARY, THEREBY IMPOSING A PRESSURE GRADIENT ON THE FLOW.
C.......THIS PARAMETER AFFECTS THE AXIAL VELOCITY AT THE UPPER BOUNDARY
C.......IN THE FOLLOWING WAY
C           U(X)= 1 + PHI*(COS((2X - L + LL)/(2LL/PI))-1)/2
C.......WHERE L IS THE LENGTH OF THE DOMAIN AND LL THE LENGTH OVER WHICH
C.......THE RETARDATION IS APPLIED. OBVIOUSLY LL<L , AND FOR RETARDATION,
C.......PHI SHOULD BE LESS THAN 1.0. LL IS REPRESENTED BY SL AND L IS
C.......REPRESENTED BY XL TO MAKE THEM REAL VARIABLES.

        PI=4.0*ATAN(1.0)

        READ(10,*)PHI
        READ(10,*)SL
        READ(10,*)XRET

C.......L IS THE HORIZONTAL DIMENSION OF THE COMPUTATIONAL DOMAIN, WHILE R
```

```
C.......IS THE VERTICAL DIMENSION (FROM THE VORTEX AXIS UP), BOTH GIVEN IN
C.......UNITS OF a (THE CORE RADIUS). R IS REPRESENTED BY RD TO AVOID
C.......REPETITION OF VARIABLES.

        READ(10,*)XL
        READ(10,*)RD
        READ(10,*)DELTAX
        READ(10,*)DELTAY

        BETA=DELTAX/DELTAY

        IF((XRET-SL/2.).LT.0.0.OR.(XRET+SL/2.).GT.XL)THEN
        WRITE(6,*)'INVALID CHOICE: CHECK DOMAIN LENGTH VS RETARD LENGHT'
        STOP
        ENDIF

C.......THE ACCELERATION PARAMETER OMEGA IS USED IN THE SUCCESIVE
C.......OVERRELAXATION METHOD. VALUE BETWEEN 1 AND 2, EXCEPT IN CASES
C.......WHERE STABILITY BECOMES A PROBLEM (CHOOSE 0.4 - 0.6)

        READ(10,*)OMEGA
        READ(10,*)MMP
        CLOSE(10)
        END

C*************************************************************************
        SUBROUTINE DOMAIN
C*************************************************************************
        INCLUDE 'NEWVRTXCOM.INC'

C.......SUBROUTINE DOMAIN CALCULATES THE DISCRETIZATION OF THE DOMAIN,
C.......OR THE VALUES OF X AND Y POINTS.

C       WRITE(6,*)'DELTAX=',DELTAX,'DELTAY=',DELTAY
        NXP=NINT(XL/DELTAX)+1
        NYP=NINT(RD/DELTAY)+1
C       WRITE(6,*)'NXP=',NXP,'NYP=',NYP
        X(1)=0.0
        Y(1)=0.0
        DO 900 I=2,NXP
            X(I)=X(I-1)+DELTAX
900     CONTINUE
        DO 950 J=2,NYP
            Y(J)=Y(J-1)+DELTAY
950     CONTINUE

C.......RESOLVE REGION NEAR THE AXIS

        DO 1000 J=2,NYP-1
            Y(J)=Y(NYP)*((LOG(Y(J)+1.)/LOG(Y(NYP)+1.))**2.2)
1000    CONTINUE
```

```
        DO 1005 J=2,NYP-1
            BETAX(J)=(Y(J)-Y(J-1))/(Y(J+1)-Y(J))
1005    CONTINUE

        BETAX(NYP)=1.0
        DJ=DELTAX/(Y(NYP)-Y(NYP-1))

        JCORE=0
        DO 1020 J=1,NYP
            IF(Y(J).LE.1.0)JCORE=JCORE+1
1020    CONTINUE

C       CALCULATION OF COORDINATES OF DISCRETE POINTS

        DO 1030 J=1,NYP
            DO 1030 I=1,NXP
                XX(I,J)=X(I)
                YY(I,J)=Y(J)
1030    CONTINUE

        END
C*******************************************************************************
        SUBROUTINE UPSTREAM
C*******************************************************************************
        INCLUDE 'NEWVRTXCOM.INC'

C.......SUBROUTINE UPSTREAM COMPUTES THE VALUES OF PSI (STREAMFUNCTION)
C.......AT X=0.0, i.e. AT THE INFLOW BOUNDARY.

        PSI(1,1)=0.0
        DO 1000 J=2,NYP
            IF(Y(J).LE.1.0)THEN
                PSI(1,J)=(Y(J)**2)*((ALPHA/2.0)+(1.0-ALPHA)*
     &              (Y(J)**2)*(3.0/2.0-(8.0/5.0*Y(J))
     &              +(1.0/2.0*(Y(J)**2))))
            ELSEIF(Y(J).GT.1.0)THEN
                PSI(1,J)=0.5*(Y(J)**2)+((ALPHA-1.0)/10.0)
            ENDIF
1000    CONTINUE
        END
C*******************************************************************************
        SUBROUTINE SIDES
C*******************************************************************************
        INCLUDE 'NEWVRTXCOM.INC'

C.......SUBROUTINE SIDES IS USED TO FIX THE VALUES OF PSI AT THE
C.......LOWER BOUNDARY, AND THE UPPER BOUNDARY IF THIS IS TO REPRESENT
C.......A SOLID BOUNDARY.

        DO 1010 I=2,NXP
            PSI(I,1)=0.0
            PSI(I,NYP)=PSI(1,NYP)
```

```
1010    CONTINUE
        END
C*************************************************************************
        SUBROUTINE INITIALIZE
C*************************************************************************
        INCLUDE 'NEWVRTXCOM.INC'

C.......SUBROUTINE INITIALIZE WILL INITIALIZE ALL POINTS OF THE DOMAIN.

        DO 1015 J=2,NYP-1
            DO 1013 I=2,NXP
                PSI(I,J)=PSI(1,J)
1013        CONTINUE
1015    CONTINUE

C.......NEED TO STORE THE VALUES OF PSI(1,J) AS A ONE DIMENSIONAL ARRAY
C.......CALLED PSII(J) TO USE IN SPLINE SUBROUTINES, AND ALSO SAVE
C.......OLD VALUES OF PSI.

        DO 1050 J=1,NYP
            PSII(J)=PSI(1,J)
1050    CONTINUE

        END
C*************************************************************************
        SUBROUTINE HEAD
C*************************************************************************
        INCLUDE 'NEWVRTXCOM.INC'

C.......SUBROUTINE HEAD COMPUTES THE TOTAL HEAD AT DISCRETIZED POINTS AS
C.......A FUNCTION OF STREAMFUNCTION PSI.

        DO 10 J=1,NYP
            IF(Y(J).LE.1.0)THEN
                H(J)=0.5*((ALPHA+(1.0-ALPHA)*(Y(J)**2)*(6.0-
     &              8.0*Y(J)+3.0*Y(J)**2))**2)+(XK**2)*(Y(J)**2)
            ELSEIF(Y(J).GT.1.0)THEN
                H(J)=0.5+(XK**2)
            ENDIF
10      CONTINUE
        END
C*************************************************************************
        SUBROUTINE CIRCULATION
C*************************************************************************
        INCLUDE 'NEWVRTXCOM.INC'

C.......SUBROUTINE CIRCULATION COMPUTES THE CIRCULATION AT DISCRETIZED
C.......POINTS AS A FUNCTION OF STREAMFUNCTION PSI.

        DO 10 J=1,NYP
            IF(Y(J).LE.1.0)THEN
                CIR(J)=XK*Y(J)**2
```

```
            ELSEIF(Y(J).GT.1.0)THEN
                CIR(J)=XK
            ENDIF
10      CONTINUE
        END
C*************************************************************************
        SUBROUTINE COMPUTATION
C*************************************************************************
        INCLUDE 'NEWVRTXCOM.INC'

        IL=2
        IU=NXP
C
        CALL CF
C
        CALL SOLVE

C       COMPUTATION OF MAXIMUM ERROR DIFFERENCE BETWEEN OLD
C       VALUES (PREVIUS ITERATION) AND NEW VALUES.

        DO 20 I=2,NXP
            EPSILON=AMAX1(EPSILON,ABS(CC(I)))
20      CONTINUE

C       STORAGE OF NEWLY COMPUTED VALUES REPLACING OLD ONES AND
C       CHECK FOR NEGATIVE VALUES OF STREAMFUNCTION PSI

        DO 22 I=2,NXP
            PSI(I,JN)= PSI(I,JN) + OMEGA*CC(I)
            IF(PSI(I,JN).LT.0.0) PSI(I,JN)=0.0
22      CONTINUE

        END
C*************************************************************************
        SUBROUTINE CF
C*************************************************************************
        INCLUDE 'NEWVRTXCOM.INC'

C                SUBROUTINE CF COMPUTES COEFFICIENT VALUES FOR THE
C                TRIDIAGONAL MATRIX TO BE USED IN THE SOLVE ALGORITHM

        IF(JN.LT.NYP)THEN
            AX=(-1.0/DELTAX**2)/( 2./DELTAX**2 + 2.*(1.+BETAX(JN))/
     &          ( BETAX(JN)*(Y(JN+1)-Y(JN))**2 + (Y(JN)-Y(JN-1))**2 ) +
     &          (1.-BETAX(JN)**2)/(Y(JN)*(Y(JN)-Y(JN-1)+(BETAX(JN)**2)*
     &          (Y(JN+1)-Y(JN)))) )
            D1= (DELTAX**2)*( 2.0/
     &          ( BETAX(JN)*(Y(JN+1)-Y(JN))**2 + (Y(JN)-Y(JN-1))**2 )+
     &          1./(Y(JN)*(Y(JN)-Y(JN-1)+(BETAX(JN)**2)*
     &          (Y(JN+1)-Y(JN)))) )
            D2= (DELTAX**2)*( 2.0*BETAX(JN)/
     &          ( BETAX(JN)*(Y(JN+1)-Y(JN))**2 + (Y(JN)-Y(JN-1))**2 ) -
```

```
     &          (BETAX(JN)**2)/(Y(JN)*(Y(JN)-Y(JN-1)+(BETAX(JN)**2)*
     &          (Y(JN+1)-Y(JN)))) )
          ELSEIF(JN.EQ.NYP)THEN
              AX=-1.0/( 2.0*(1.0+(DELTAX/(Y(JN)-Y(JN-1)))**2) )
              D3=(DELTAX**2)*( 2.*Y(JN)/(Y(JN)-Y(JN-1)) - 1.0)
          ENDIF
C
          DD(2)=1.0
          AA(2)=AX
          DO 15 I=3,IU-1
              BB(I)=AX
              DD(I)=1.0
              AA(I)=AX
15        CONTINUE
          DD(IU)=1.0
          BB(IU)=2.0*AX
          DO 25 I=2,IU
              RR=PSI(I,JN)
              IF(RR.LT.PSII(JCORE))THEN
                  CX(I)=SEVAL(RR,CIR,DC,PSII,JCORE)
                  DCC(I)=DEVAL(RR,CIR,DC,PSII,JCORE)
                  DHH(I)=DEVAL(RR,H,DH,PSII,JCORE)
C           USE NEXT ONLY IF PROFILE IS RADIALLY INVARIANT.
              ELSEIF(RR.GE.PSII(JCORE))THEN
                  CX(I)=0.0
                  DCC(I)=0.0
                  DHH(I)=0.0
              ENDIF
C           OTHERWISE, USE THE FOLLOWING:
C           CX(I)=SEVAL(RR,CIR,DC,PSII,NYP)
C           DCC(I)=DEVAL(RR,CIR,DC,PSII,NYP)
C           DHH(I)=DEVAL(RR,H,DH,PSII,NYP)
              BX=((Y(JN)**2)*DHH(I) - CX(I)*DCC(I))*
     &             (DELTAX**2)
C
C
              IF(I.LT.NXP.AND.JN.LT.NYP)THEN
                  CC(I)=AX*(BX-(D2*PSI(I,JN+1)+D1*PSI(I,JN-1)) )
     &                 -AX*PSI(I+1,JN)-AX*PSI(I-1,JN)-PSI(I,JN)
              ELSEIF(I.LT.NXP.AND.JN.EQ.NYP)THEN
               IF(PHI.LT.1.0E-05)THEN
                CC(I)=AX*(BX - 2.0*(DJ**2)*PSI(I,JN-1)
     &               -1.0*D3)
     &               - AX*PSI(I-1,JN)-AX*PSI(I+1,JN) - PSI(I,JN)
               ELSEIF(PHI.GE.1.0E-05)THEN
                IF(X(I).LE.(XRET-SL/2.))THEN
                  CC(I)=AX*(BX - 2.0*(DJ**2)*PSI(I,JN-1)-1.0*D3)
     &                 - AX*PSI(I-1,JN)-AX*PSI(I+1,JN)-PSI(I,JN)
             ELSEIF(X(I).GT.((XRET-SL/2.)).AND.X(I).LT.((XRET+SL/2.)))THEN
                  CC(I)=AX*(BX - 2.0*(DJ**2)*PSI(I,JN-1) -
     &              D3*(1.0+PHI*(COS((X(I)+SL/2.-XRET)/(SL/PI))-1.)/2.))
     &              -AX*PSI(I+1,JN) -AX*PSI(I-1,JN) - PSI(I,JN)
```

```
            ELSEIF(X(I).GE.(XRET+SL/2.))THEN
              CC(I)=AX*(BX - 2.0*(DJ**2)*PSI(I,JN-1)-(1.0-PHI)*D3)
     &              - AX*PSI(I-1,JN)-AX*PSI(I+1,JN) - PSI(I,JN)
            ENDIF
           ENDIF
          ELSEIF(I.EQ.NXP.AND.JN.LT.NYP)THEN
             CC(I)=AX*(BX-(D2*PSI(I,JN+1)+D1*PSI(I,JN-1)))
     &            -2.*AX*PSI(I-1,JN)-PSI(I,JN)
          ELSEIF(I.EQ.NXP.AND.JN.EQ.NYP)THEN
              IF(PHI.LT.1.0E-05)THEN
                  CC(I)=AX*(BX - 2.0*(DJ**2)*PSI(I,JN-1)
     &                -1.0*D3)
     &                - 2.*AX*PSI(I-1,JN)- PSI(I,JN)
              ELSEIF(PHI.GE.1.0E-05)THEN
                  CC(I)=AX*(BX - 2.0*(DJ**2)*PSI(I,JN-1)
     &                -(1.0-PHI)*D3)
     &                - 2.*AX*PSI(I-1,JN)- PSI(I,JN)
              ENDIF
          ENDIF
25      CONTINUE
        END

C*************************************************************************
        SUBROUTINE SOLVE
C*************************************************************************
        INCLUDE 'NEWVRTXCOM.INC'
C.......SUBROUTINE SOLVE SOLVES TRIDIAGONAL SYSTEM BY ELIMINATION
C.......IL=SUBSCRIPT OF FIRST EQUATION
C.......IU=SUBSCRIPT OF LAST EQUATION
C.......BB=COEFFICIENT BEHIND DIAGONAL
C.......DD=COEFFICIENT ON DIAGONAL
C.......AA=COEFFICIENT AHEAD OF DIAGONAL
C.......CC=ELEMENT OF CONSTANT VECTOR
C
C.......ESTABLISH UPPER TRIANGULAR MATRIX
C
        LP=IL+1
        DO 10 I=LP,IU
            R=BB(I)/DD(I-1)
            DD(I)=DD(I)-R*AA(I-1)
            CC(I)=CC(I)-R*CC(I-1)
10      CONTINUE
C.......BACKSUBSTITUTION
        CC(IU)=CC(IU)/DD(IU)
        DO 20 I=LP,IU
            JJ=IU-I+IL
            CC(JJ)=(CC(JJ)-AA(JJ)*CC(JJ+1))/DD(JJ)
20      CONTINUE
C.......SOLUTION STORED IN CC
        RETURN
        END
C*************************************************************************
```

```
      SUBROUTINE VELOCITY
C*********************************************************************
      INCLUDE 'NEWVRTXCOM.INC'

C     COMPUTE AXIAL, RADIAL, CIRCUMFERENTIAL VELOCITIES

      DO 27 J=2,NYP-1
          DO 27 I=2,NXP-1

C               CALCULATION OF AXIAL AND RADIAL VELOCITIES FROM
C               STREAMFUNCTION VALUES.

            U(I,J)=(1./Y(J))*( PSI(I,J)-PSI(I,J-1)+(BETAX(J)**2)*
     &             (PSI(I,J+1)-PSI(I,J)) )/( Y(J)-Y(J-1) +
     &             (BETAX(J)**2)*(Y(J+1)-Y(J)) )
            V(I,J)=(-1./Y(J))*(PSI(I+1,J)-PSI(I-1,J))/(2.*DELTAX)
 27   CONTINUE

      THETA1=(Y(2)-Y(1))/(Y(3)-Y(2))
      THETA2=(Y(NYP)-Y(NYP-1))/(Y(NYP-1)-Y(NYP-2))
      THETA1=THETA1/(1.+THETA1)
      THETA2=THETA2/(1.+THETA2)

      DO 28 I=1,NXP
        U(I,1)=2.0*PSI(I,2)/(Y(2)**2)
        U(I,NYP)=(1./Y(NYP))*( PSI(I,NYP-1)+
     &           (THETA2**2-1.)*PSI(I,NYP)-(THETA2**2)*PSI(I,NYP-2))/
     &           ( (Y(NYP)-Y(NYP-1))*(THETA2-1.) )
        V(I,1)=0.0
 28   CONTINUE

      DO 29 J=2,NYP
        V(1,J)=(-1./Y(J))*(-3.*PSI(1,J)+4.*PSI(2,J)-PSI(3,J))/
     &         (2.0*DELTAX)
        V(NXP,J)=(-1./Y(J))*(3.*PSI(NXP,J)-4.*PSI(NXP-1,J)+
     &           PSI(NXP-2,J))/(2.0*DELTAX)
 29   CONTINUE

      DO 30 J=2,NYP-1
        U(1,J)=(1./Y(J))*( PSI(1,J)-PSI(1,J-1)+(BETAX(J)**2)*
     &         (PSI(1,J+1)-PSI(1,J)) )/( Y(J)-Y(J-1) +
     &         (BETAX(J)**2)*(Y(J+1)-Y(J)) )
        U(NXP,J)=(1./Y(J))*( PSI(NXP,J)-PSI(NXP,J-1)+(BETAX(J)**2)*
     &           (PSI(NXP,J+1)-PSI(NXP,J)) )/( Y(J)-Y(J-1) +
     &           (BETAX(J)**2)*(Y(J+1)-Y(J)) )
 30   CONTINUE

      DO 31 I=2,NXP-1
        V(I,NYP)=(-1./Y(NYP))*(PSI(I+1,NYP)-PSI(I-1,NYP))/
     &           (2.*DELTAX)
 31   CONTINUE
```

```
      DO 34 I=1,NXP
       DO 34 J=1,NYP

C              CALCULATION OF CIRCUMFERENTIAL VELOCITY USING CIRCULATION
C              VALUES AT DISCRETE POINTS.

               RRR=PSI(I,J)
               IF(J.EQ.1)THEN
                   W(I,J)=0.0
               ELSEIF(J.GT.1)THEN
                   W(I,J)=SEVAL(RRR,CIR,DC,PSII,NYP)/Y(J)
               ENDIF

C               CALCULATION OF TOTAL HEAD AND CIRCULATION USING PSI(I,J)

            CIRCLN(I,J)=SEVAL(RRR,CIR,DC,PSII,NYP)
            TOTHEAD(I,J)=SEVAL(RRR,H,DH,PSII,NYP)

C               CALCULATION OF TOTAL VELOCITY FROM AXIAL,RADIAL AND
C               CIRCUMFERENTIAL VELOCITIES COMPUTED ABOVE.

             TOTVEL(I,J)=SQRT(U(I,J)**2+V(I,J)**2+W(I,J)**2)

C               CALCULATION OF TOTAL PRESSURE FROM HEAD AND TOTAL VELOCITY

             PRESSR(I,J)=SEVAL(RRR,H,DH,PSII,NYP)-
     +                   0.5*(TOTVEL(I,J)**2)
 34    CONTINUE

       DO 46 I=1,NXP
           UO(I)=U(I,1)
           UO2(I)=U(I,NYP)
           VTOP(I)=V(I,NYP)
           VTOP2(I)=V(I,NYP-1)
           VAXIS(I)=V(I,2)
46     CONTINUE
C
C      FIND CORE EDGE LOCATION AFTER EXPANSION : Y(JCOREB)
C
       RR=0.5+((ALPHA-1.0)/10.0)
       ETA1=100.
       DO 47 J=1,NYP
           RRR=ABS(RR-PSI(NXP,J))
           ETA2=AMIN1(ETA1,RRR)
           IF(ETA2.EQ.RRR)THEN
             JCOREB=J
             ETA1=ETA2
           ENDIF
 47    CONTINUE

       DO 48 J=1,JCOREB
           Z(J)=Y(J)
```

```
          Z(J+JCOREB)=Y(J)
 48     CONTINUE

        DO 49 J=1,NYP
            UINIT(J)=U(1,J)
            UMID4(J)=U(NXP/4,J)
            UMID38(J)=U(3*NXP/8,J)
            UMID2(J)=U(NXP/2,J)
            UMID58(J)=U(5*NXP/8,J)
            UMID34(J)=U(3*NXP/4,J)
            UEND(J)=U(NXP,J)
            U2(J)=U(2,J)
            U3(J)=U(NXP-1,J)
            WINIT(J)=W(1,J)
            WMID4(J)=W(NXP/4,J)
            WMID38(J)=W(3*NXP/8,J)
            WMID2(J)=W(NXP/2,J)
            WMID58(J)=W(5*NXP/8,J)
            WMID34(J)=W(3*NXP/4,J)
            WEND(J)=W(NXP,J)
 49     CONTINUE
 C
 C      USE BATCHELOR SOLUTION TO COMPARE WITH NUMERICAL SOLUTION
 C
        XKB=2.0*XK*Y(JCOREB)
        WRITE(6,*)'THE CORE EXPANSION IS=',Y(JCOREB)
        DO 50 J=1,JCOREB
            UBESS(J)=UEND(J)
            WBESS(J)=WEND(J)
 50     CONTINUE
        BEJ1=BESSJ1(XKB)
        DO 51 J=JCOREB+1,2*JCOREB
            XKY=2.0*XK*Y(J-JCOREB)
            BEJO=BESSJO(XKY)
            UBESS(J)=1.+(1./(Y(JCOREB)**2)-1.)*(XK*Y(JCOREB)*BEJO/BEJ1)
            WEJ1=BESSJ1(XKY)
            WBESS(J)=XK*(Y(J-JCOREB)+(1./Y(JCOREB)**2 -1.)*
     +              Y(JCOREB)*(WEJ1/BEJ1))
 51     CONTINUE

        DO 60 J=1,NYP
           UGEN(J)=UINIT(J)
           UGEN(J+NYP)=UMID4(J)
           UGEN(J+2*NYP)=UMID38(J)
           UGEN(J+3*NYP)=UMID2(J)
           UGEN(J+4*NYP)=UMID58(J)
           UGEN(J+5*NYP)=UMID34(J)
           UGEN(J+6*NYP)=UEND(J)
           WGEN(J)=WINIT(J)
           WGEN(J+NYP)=WMID4(J)
           WGEN(J+2*NYP)=WMID38(J)
           WGEN(J+3*NYP)=WMID2(J)
```

```
          WGEN(J+4*NYP)=WMID58(J)
          WGEN(J+5*NYP)=WMID34(J)
          WGEN(J+6*NYP)=WEND(J)
60      CONTINUE

        DO 65 J=1,NYP
          PRS(J)=PRESSR(1,J)
          PRS(J+NYP)=PRESSR(NXP/4,J)
          PRS(J+2*NYP)=PRESSR(3*NXP/8,J)
          PRS(J+3*NYP)=PRESSR(NXP/2,J)
          PRS(J+4*NYP)=PRESSR(5*NXP/8,J)
          PRS(J+5*NYP)=PRESSR(3*NXP/4,J)
          PRS(J+6*NYP)=PRESSR(NXP,J)
          YGEN(J)=Y(J)
          YGEN(J+NYP)=Y(J)
          YGEN(J+2*NYP)=Y(J)
          YGEN(J+3*NYP)=Y(J)
          YGEN(J+4*NYP)=Y(J)
          YGEN(J+5*NYP)=Y(J)
          YGEN(J+6*NYP)=Y(J)
65      CONTINUE



C       COMPUTE EXACT AXIAL VELOCITY AT UPPER EDGE

        DO 100 I=1,NXP
            IF(X(I).LE.(XRET-SL/2.))THEN
                UTOP(I)=1.0
            ELSEIF(X(I).GT.((XRET-SL/2.)).AND.X(I).LT.((XRET+SL/2.)))THEN
                UTOP(I)=1.0+PHI*(COS((X(I)+SL/2.-XRET)/(SL/PI))-1.)/2.
            ELSEIF(X(I).GE.(XRET+SL/2.))THEN
                UTOP(I)=1.0-PHI
            ENDIF
100     CONTINUE

        RETURN
        END

C*******************************************************************************
        SUBROUTINE PLOT
C*******************************************************************************
        INCLUDE 'NEWVRTXCOM.INC'

C       THIS SUBROUTINE STORES DATA TO BE USED IN PLOTTING.

        OPEN(UNIT=9,FILE='COORDINT.DAT',STATUS='UNKNOWN')
        DO 34 I=1,NXP
          WRITE(9,*)X(I)
34      CONTINUE
        DO 35 J=1,NYP
          WRITE(9,*)Y(J)
```

```
 35     CONTINUE
        CLOSE(9)
C
        OPEN(UNIT=11,FILE='STRMFNCTN.DAT',STATUS='UNKNOWN')
        DO 37 J=1,NYP
            DO 36 I=1,NXP
                WRITE(11,*)PSI(I,J),YY(I,J),XX(I,J)
36          CONTINUE
37      CONTINUE
        CLOSE(11)
C
        OPEN(UNIT=12,FILE='VELOCITY.DAT',STATUS='UNKNOWN')
        DO 47 J=1,NYP
            DO 47 I=1,NXP
                WRITE(12,*)U(I,J),V(I,J),W(I,J),YY(I,J),XX(I,J)
47      CONTINUE
        CLOSE(12)
C
        OPEN(UNIT=13,FILE='CIRCLN.DAT',STATUS='UNKNOWN')
        DO 55 J=1,NYP
           DO 50 I=1,NXP
              WRITE(13,*)CIRCLN(I,J),YY(I,J),XX(I,J)
 50        CONTINUE
 55     CONTINUE
        CLOSE(13)
C
        OPEN(UNIT=14,FILE='PROFILE.DAT',STATUS='UNKNOWN')
           DO 60 J=1,7*NYP
              WRITE(14,*)PRS(J),UGEN(J),WGEN(J),YGEN(J)
 60     CONTINUE
        CLOSE(14)
C
        OPEN(UNIT=15,FILE='JUSTRUN.DAT',STATUS='UNKNOWN')
        WRITE(15,*)ALPHA,MP,NNN,XK,PHI,SL,DELTAX,DELTAY,NXP,NYP,EPSILON
        CLOSE(15)
C
        OPEN(UNIT=16,FILE='ERROR.DAT',STATUS='UNKNOWN')
          DO 70 I=0,MP
            WRITE(16,*)EPS(I)
 70       CONTINUE
        CLOSE(16)
C
        RETURN
        END

C*********************************************************************
        SUBROUTINE SPLINE(XV,XS,S,N)
C*********************************************************************

C.......SUBROUTINE SPLINE USED FOR BOTH HEAD AND CIRCULATION

        INTEGER N
```

```
      DIMENSION XV(N),XS(N),S(N)
      DIMENSION A(500),B(500),C(500)
      REAL DSM,DSP
C-----------------------------------------------------
C     Calculates spline coefficients for XV(S).      |
C     To evaluate the spline at some value of S,     |
C     use SEVAL and/or DEVAL.                        |
C                                                    |
C     S       independent variable array (input)     |
C     XV      dependent variable array   (input)     |
C     XS      dXV/dS array               (calculated)|
C     N       number of points           (input)     |
C                                                    |
C-----------------------------------------------------
C

C

      IF(N.GT.500) STOP 'SPLINE: array overflow'
C
      DO 1 I=2, N-1
          DSM = S(I) - S(I-1)
          DSP = S(I+1) - S(I)
          B(I) = DSP
          A(I) = 2.0*(DSM+DSP)
          C(I) = DSM
          XS(I) = 3.0*((XV(I+1)-XV(I))*DSM/DSP+(XV(I)-XV(I-1))*DSP/DSM)
1     CONTINUE
C
C---- set specified first derivative end conditions
C     XS1 = 0.
C     XS2 = 0.
C     A(1) = 1.0
C     C(1) = 0.
C     XS(1) = XS1
C     A(N) = 1.0
C     B(N) = 0.
C     XS(N) = XS2
C
C---- set zero second derivative end conditions
      A(1) = 2.0
      C(1) = 1.0
      XS(1) = 3.0*(XV(2)-XV(1)) / (S(2)-S(1))
      B(N) = 1.0
      A(N) = 2.0
      XS(N) = 3.0*(XV(N)-XV(N-1)) / (S(N)-S(N-1))
C
      CALL TRISOL(A,B,C,XS,N)
      RETURN
      END ! SPLINE
```

```
      SUBROUTINE TRISOL(A,B,C,D,KK)
      INTEGER KK
      DIMENSION A(KK),B(KK),C(KK),D(KK)
C---------------------------------------
C     Solves KK long, tri-diagonal system |
C                                         |
C           A C          D                |
C           B A C        D                |
C             B A .      .                |
C               . . C    .                |
C                 B A    D                |
C                                         |
C     The righthand side D is replaced by |
C     the solution.  A, C are destroyed.  |
C---------------------------------------
C
      DO 1 K=2, KK
          KM = K-1
          C(KM) = C(KM) / A(KM)
          D(KM) = D(KM) / A(KM)
          A(K) = A(K) - B(K)*C(KM)
          D(K) = D(K) - B(K)*D(KM)
1     CONTINUE
C
      D(KK) = D(KK)/A(KK)
C
      DO 2 K=KK-1, 1, -1
          D(K) = D(K) - C(K)*D(K+1)
2     CONTINUE
C
      RETURN
      END ! TRISOL


      FUNCTION SEVAL(SS,XV,XS,S,N)
      INTEGER N
      DIMENSION XV(N), XS(N), S(N)
      REAL SS,DS,CX1,CX2,T
C-------------------------------------------------
C     Calculates XV(SS)                           |
C     XS array must have been calculated by SPLINE |
C-------------------------------------------------
      ILOW = 1
      II = N
C
10    IF(II-ILOW .LE. 1) GO TO 11
C
      IMID = (II+ILOW)/2
      IF(SS .LT. S(IMID)) THEN
          II = IMID
      ELSE
          ILOW = IMID
```

```
        ENDIF
        GO TO 10
C
11      DS = S(II) - S(II-1)
        T = (SS - S(II-1)) / DS
        CX1 = DS*XS(II-1) - XV(II) + XV(II-1)
        CX2 = DS*XS(II) - XV(II) + XV(II-1)
        SEVAL = T*XV(II)+(1.0-T)*XV(II-1)+(T-T*T)*((1.0-T)*CX1 - T*CX2)
        RETURN
        END ! SEVAL


        FUNCTION DEVAL(SS,XV,XS,S,N)
        INTEGER N
        DIMENSION XV(N), XS(N), S(N)
C-----------------------------------------------
C     Calculates dXV/dS(SS)                     |
C     XS array must have been calculated by SPLINE |
C-----------------------------------------------
        ILOW = 1
        II = N
C
10      IF(II-ILOW .LE. 1) GO TO 11
C
        IMID = (II+ILOW)/2
        IF(SS .LT. S(IMID)) THEN
            II = IMID
        ELSE
            ILOW = IMID
        ENDIF
        GO TO 10
C
11      DS = S(II) - S(II-1)
        T = (SS - S(II-1)) / DS
        CX1 = DS*XS(II-1) - XV(II) + XV(II-1)
        CX2 = DS*XS(II) - XV(II) + XV(II-1)
        DEVAL = XV(II)-XV(II-1)+(1.-4.0*T+3.0*T*T)*CX1+T*(3.0*T-2.)*CX2
        DEVAL = DEVAL/DS
        RETURN
        END ! DEVAL
C*********************************************************************
        FUNCTION BESSJ1(X)
C*********************************************************************
C         Function returns the Bessel function J1(x) for any real x
        REAL*8 Y,P1,P2,P3,P4,P5,Q1,Q2,Q3,Q4,Q5,R1,R2,R3,R4,R5,R6
     *       S1,S2,S3,S4,S5,S6
        DATA R1,R2,R3,R4,R5,R6/72362614232.D0,-7895059235.D0,
     *       242396853.1D0,-2972611.439D0,15704.48260D0,-30.16036606D0/,
     *       S1,S2,S3,S4,S5,S6/144725228442.D0,2300535178.D0,
     *       18583304.74D0,99447.43394D0,376.9991397D0,1.D0/
        DATA P1,P2,P3,P4,P5/1.D0,.183105D-2,-.3516396496D-4,
     *       .2457520174D-5,-.240337019D-6/,Q1,Q2,Q3,Q4,Q5/
```

```
     *       .04687499995D0,-.2002690873D-3,.8449199096D-5,
     *       -.88228987D-6,.105787412D-6/
C          Direct Rational Approximation
           IF(ABS(X).LT.8.)THEN
              Y=X**2
              BESSJ1=X*(R1+Y*(R2+Y*(R3+Y*(R4+Y*(R5+Y*R6)))))/
     *             (S1+Y*(S2+Y*(S3+Y*(S4+Y*(S5+Y*S6)))))
           ELSE
              DX=ABS(X)
              Z=8./DX
              Y=Z**2
              XX=DX-2.356194491
              BESSJ1=SQRT(0.636619772/DX)*(COS(XX)*(P1+Y*(P2+Y*(P3+Y*
     *             (P4+Y*P5))))-Z*SIN(XX)*(Q1+Y*(Q2+Y*(Q3+Y*
     *             (Q4+Y*Q5)))))*SIGN(1.,X)
           ENDIF
           RETURN
           END
C*********************************************************************
           FUNCTION BESSJ0(X)
C*********************************************************************
C            Returns the Bessel function J0(X) for any real x
           REAL*8 Y,P1,P2,P3,P4,P5,Q1,Q2,Q3,Q4,Q5,R1,R2,R3,R4,R5,R6
     *       S1,S2,S3,S4,S5,S6
           DATA P1,P2,P3,P4,P5/1.D0,-.1098628627D-2,.2734510407D-4,
     *       -.2073370639D-5,.2093887211D-6/,Q1,Q2,Q3,Q4,Q5/
     *       -.1562499995D-1,.1430488765D-3,-.6911147651D-5,
     *       .7621095161D-6,-.934945152D-7/
           DATA R1,R2,R3,R4,R5,R6/57568490574.D0,-13362590354.D0,
     *       651619640.7D0,-11214424.18D0,77392.33017D0,
     *       -184.9052456D0/,S1,S2,S3,S4,S5,S6/57568490411.D0,
     *       1029532985.D0,9494680.718D0,59272.64853D0,
     *       267.8532712D0,1.D0/
C          Direct Rational Function Fit
           IF(ABS(X).LT.8.)THEN
              Y=X**2
              BESSJ0=(R1+Y*(R2+Y*(R3+Y*(R4+Y*(R5+Y*R6)))))/
     *             (S1+Y*(S2+Y*(S3+Y*(S4+Y*(S5+Y*S6)))))
           ELSE
              DX=ABS(X)
              Z=8./DX
              Y=Z**2
              XX=DX-.785398164
              BESSJ0=SQRT(.636619772/DX)*(COS(XX)*(P1+Y*(P2+Y*
     *             (P3+Y*(P4+Y*P5))))-Z*SIN(XX)*(Q1+Y*(Q2+Y*
     *             (Q3+Y*(Q4+Y*Q5)))))
           ENDIF
           RETURN
           END
C********* ********* ********* ********* ********* ********* ********* *
```